UNIVERSITY OF CALGARY

Discrete Sliding Mode Control of Magnetic Bearings

by

Shane Edmonds

A THESIS

SUBMITTED TO THE FACULTY OF GRADUATE STUDIES

IN PARTIAL FULFILMENT OF THE REQUIREMENTS FOR THE

DEGREE OF MASTER OF APPLIED SCIENCE

DEPARTMENT OF MECHANICAL ENGINEERING

CALGARY, ALBERTA

NOVEMBER, 1999

Abstract

Magnetic bearings are capable of suspending shafts rotating at high speed without mechanical contact or lubrication, providing many advantages and opportunities in industrial and medical applications. A formidable control problem is presented by their fast, interactive and unstable multivariable dynamics. This thesis provides methods for designing controllers for magnetic bearings along with their experimental evaluation.

In a novel approach, the experimental apparatus was modeled using a parameter estimation method calculated from input and output data. An optimal controller and a discrete sliding mode controller with outer-loop integration were designed. A sliding mode controller was also implemented that changed the sliding surface depending on shaft position to more aggressively achieve the performance objective of preventing shaft mechanical touchdown. Experimental testing verified the tuning goal and showed that the sliding mode controllers with guaranteed robustness performed comparably in disturbance rejection to the optimal controllers. This work summarizes conditions for controller selection.

Acknowledgments

I would like to thank Dr. Pieper for his support and guidance in undertaking the work presented in this thesis.

Table of Contents

List of Tables

List of Figures

List of Symbols

$0_{i \times j}$	Zero matrix with i rows and j columns
C	Sliding surface matrix
E	Expectation operator
H	Output matrix of a model
h, v	Subscript, referring to horizontal or vertical axis
I_n	Identity matrix of size $n \times n$
J	Cost function
k	Time step in a discrete plant. $(Time = k.T)$
l, r	Subscript, referring to left or right shaft end
q^{-1}	Unit delay operator
T	Sample period (seconds)
u	Input to the plant (control signal)
x	State vector of the model
$\hat{x}$	Estimate of state vector of a model
y	Output of the plant
Φ	State transition matrix of a model
Γ	Input matrix of a model

List of Abbreviations

ADC	Analog to Digital Converter
AMB	Active Magnetic Bearing
DAC	Digital to Analog Converter
DSMC	Discrete Sliding Mode Control
DSP	Digital Signal Processor
LQG	Linear Quadratic Gaussian
PC	Personal Computer
PD	Proportional, Derivative Controller
PI	Proportional, Integral Controller
PID	Proportional, Integral, Derivative Controller
MIMO	Multiple-Input, Multiple-Output
RMS	Root Mean Squared
SISO	Single-Input, Single-Output

Chapter 1
Introduction

Active Magnetic Bearings (AMB) act to levitate a shaft and allow it to rotate without contact. This feature creates advantages for many applications due to lower rotation friction in bearings and the ability to achieve active vibration damping. Magnetic bearings are currently used in many applications with others under investigation, for example in natural gas compressors in remote locations where their higher rotating efficiency and reduced maintenance requirements make them ideal.

A typical AMB consists of four electromagnets positioned equidistant around the shaft to be supported. Sensors adjacent to the electromagnets monitor the relative horizontal and vertical position of the shaft and a controller continuously adjusts the magnetic fields to maintain the required shaft positioning. This controller must have a very high response capability due to the potential high rotational speed of the shaft and its intrinsic instability. Usually one AMB is located at each end of the shaft.

The reduced losses allow faster rotation of the shaft resulting in increased efficiency in most applications. The ends of a shaft using AMBs can also be continuously realigned for such applications as a fast conveyor. A particular feature of an AMB is the ability to provide dynamic damping of vibrations caused by unavoidable shaft imbalances. This is due to the ability of the shaft to be rotated around its centre of mass within the magnetic

field of the bearing (as compared with a conventional bearing which restricts the shaft to rotate around its geometric centre).

A shaft levitated by magnets, due to its operating principles, is unstable and the magnetic fields must be continuously modified by a controller to keep the shaft in place. In principle this is similar to keeping a pen standing upright on the palm of your hand in that without active control, the pen will surely topple. High operating speeds and the fact that there are several magnets required to keep the shaft levitated make the control of magnetic bearings an interesting and formidable problem.

The solution to this problem requires the measurement of the shaft position and an active controller. Ideally the controller should keep the shaft levitated at all times but this is not feasible since the controller must respond with a strength appropriate to the given conditions. If, for example, the mass of the shaft changes (due to deposits or parts breaking off) then a different actuation level is required for corrective action. If this mass change is not known then the controller may not be tuned appropriately. This can result in the shaft falling and hitting the supporting frame. A measure of how well a controller performs can be made by testing the conditions which cause it to fail. A more robust controller has a larger variation in conditions under which it is stable.

In this work, controllers have been designed and tested for an AMB apparatus with particular interest in the system stability and the ability of the controller to maintain the shaft within certain deviation limits so as not to hit the bearing frame. In particular, a sliding mode control approach was used. AMBs are currently being used in a number of practical applications and this development has the potential to increase the opportunity

for further such applications through the novel modeling method and robust control law application presented in this work. It is anticipated that the controller as developed could increase the potential range of applications of AMBs in industry.

1.1 Contributions of this Thesis

This thesis provides a method for designing and implementing digital controllers for magnetic bearing systems. Specifically the main contributions are:

- A model of a magnetic bearing was produced using the method of parameter estimation which is derived from data rather than physical principles. This appears to be a novel method of modeling a magnetic bearing.
- A Linear Quadratic Gaussian controller with three different tuning parameters was designed. Tests verify the goal of the tuning.
- A Discrete Sliding Mode Controller was designed with an optimal sliding surface. This controller was tested with three sliding surfaces and the tuning goal was verified. This control law has not been applied to a magnetic bearing in the literature. The controller was stable using a relatively slow sampling rate thus reduced computational load.
- A Proportional-Integral controller was combined with the Discrete Sliding Mode Controller and the tracking performance was demonstrated.
- A Discrete Sliding Mode Controller was designed with a choice of sliding surface dependant on the position of the shaft. This appeared to be a novel and promising controller but the test results produced mixed performance.

- Following a tap disturbance to the shaft, the Discrete Sliding Mode Controller returned the shaft to its normal position faster than the Linear Quadratic Gaussian controller.

This thesis provides guidelines for future applications of digital controllers to Active Magnetic Bearings.

1.2 Organization of this Thesis

The organization of the seven chapters of this thesis follows the sequence of experimental development.

Chapter Two explains the motivation for the use of magnetic bearings and illustrates some applications. The operation and available modeling methods are discussed. Several different control algorithms including sliding mode control are outlined along with their established performance results.

Chapter Three describes the apparatus and control hardware and software used for the experiments.

Chapter Four presents the different methods attempted for producing a model of the apparatus. A physical principles analysis is first discussed followed by an attempt to derive a model from the closed loop frequency response. The method of least squares parameter estimation is explained and applied. The resulting model with a novel refinement for resonant mode enhancement is then presented.

Chapter Five details the design procedures for the controllers. Specifically, a Linear Quadratic Gaussian and a Discrete Sliding Mode Controller are designed and tuned for specific performance objectives.

Chapter Six presents the experimental results of tests performed with the controllers designed in Chapter Five. Several different tests were performed using different tuning constants and the results were compared to evaluate the effect of the tuning.

Chapter Seven contains a summary of the main results and some direction for future work.

Chapter 2
Background Information

Magnetic bearings are capable of suspending rotating shafts at high speeds without mechanical contact with the supporting structure. They offer many advantages over conventional bearings including (Knospe & Collins, 1996):

- lower rotating losses
- possibility of active vibration damping
- higher speeds
- elimination of lubrication systems and lubricant contamination of the system
- operation at temperature extremes and in a vacuum
- longer lifetime

They are presently used in many applications such as industrial, medical, military and space applications including pumps, compressors, flywheels, grinding and milling spindles, turbine engines and centrifuges (Knospe & Collins, 1996). Turbomachines such as gas turbines, jet engines, pumps and compressors operate at high speeds to achieve desired efficiency but roller bearings have a relatively short life-span and although fluid film bearings have a longer life-span they require an extensive oil supply system and seals (Humphris et al, 1986). In the future demand for greater speed, for example in an energy

storage flywheel (as in Ahrens et al, 1996), will likely lead to more demanding applications of magnetic bearings.

Magnetic bearings require a solution to a difficult control problem due to their fast open loop unstable and interactive multiple input, multiple output (MIMO) nature. The dynamics of a shaft levitated with magnetic bearings inherently contain non-linearities and change with increasing rotational speeds especially near the critical frequencies of the shaft. All rotating machinery also has some residual imbalance which must be dealt with by the controller. The controller can offer the ability for shaft positioning and alignment as well as diagnostic and load measurement capabilities (Knospe & Collins, 1996).

2.1 Operation of Active Magnetic Bearings

The conventional design of a magnetic bearing consists of a separate magnetic actuator component shown in Figure 2.1 and a corresponding position sensor component located near the actuator. The horizontally opposed pair of horseshoe magnets attracts the shaft to the right by adding the current I_x to a bias (or steady state level) current, i_0, in the right magnet while reducing the bias current in the left magnet by i_x. In an analogous way the shaft can be attracted in a vertical direction. The contact-free position sensor measures the horizontal and vertical gap width. The attractive force of the magnets is inversely proportional to the gap width squared resulting in an unstable plant.

The gap magnetic flux exerts a force on the shaft and is proportional to the current squared. With little current flowing the force cannot be changed quickly due to a slow force to current slew rate (Bleuler et al, 1994; Charara et al, 1996; Knospe & Collins,1996;

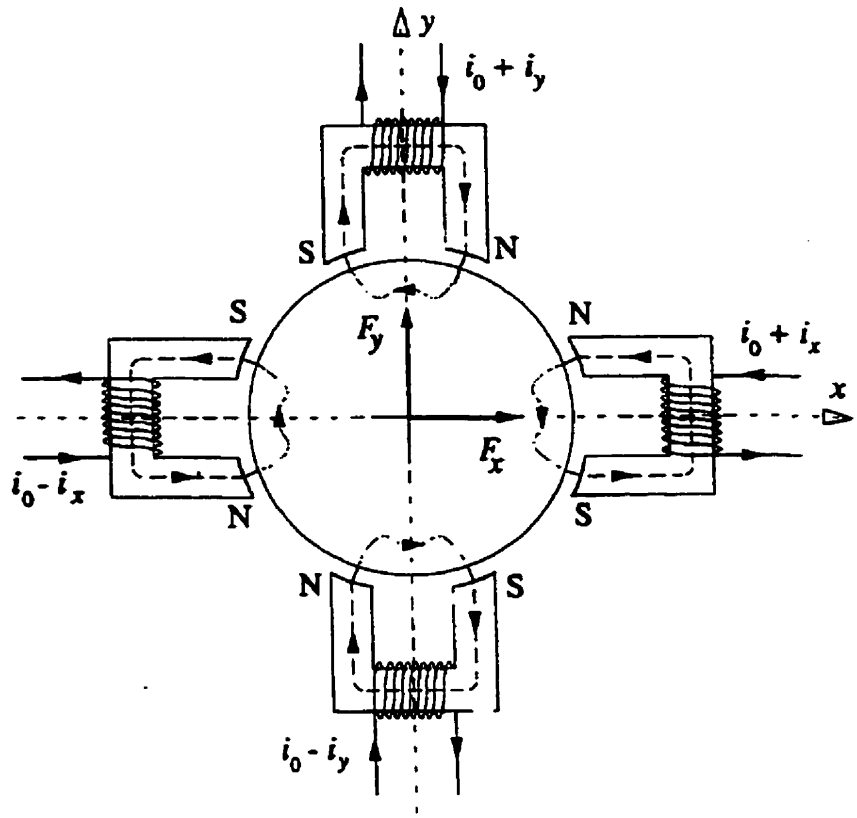

Figure 2.1 End View of One Magnetic Bearing (Lum et al, 1996)

Mizuno et al, 1996). Thus a bias current, i_0, equal to half of the rated current, i_{max}, is usually run through the coils so changes to the flux are made around this operating point. This provides a much larger force slew rate (Knospe & Collins, 1996) and allows a model of the plant to be linearized for small perturbations around the operating point (Lum et al, 1996; Matsumura & Yoshimoto, 1986). The total current in each pair of magnets is always $i_{\max}$ ($i_{Total} = i_0 + i_x + i_0 - i_x = 2i_0 = i_{\max}$). The bias current exerts no net force on the shaft but produces a constant magnetic field. A current is induced in the shaft due to its relative motion with the magnetic field of the bias current. This results in a larger electromagnetic

drag than with no bias current when rotating. Experiments in Charara et al, 1996 without a bias current demonstrated that the rotor vibration and energy consumption of the bearing are lower using a non-linear control law. A magnetic bearing without a bias current has the potential for a greater operating efficiency at the cost of a slower force to current slew rate.

Recently there has been research into self-sensing magnetic bearings that do not have a separate position sensor but deduce the gap width from the actuator currents and/or actuator gap flux measurements (Bleuler et al, 1994). This reduces the cost and complexity of the bearing and the actuator and sensor are inherently collocated. An estimator based on only the actuator current information is also presented. A full order and reduced order gap estimator was presented in Mizuno et al, 1996. A gap parameter estimation method was developed in Noh & Maslen, 1997 and demonstrated stable experimental results.

The magnetic bearing controller must use the position measurements or estimates to adjust the current in the magnets and keep the shaft at the required position. The rotating shaft will always have some residual imbalance following a mechanical balancing procedure. This can either be compensated for by electromagnetic forces in an attempt to rotate the shaft about its geometric center or the shaft can rotate around its axis of inertia. The latter control strategy referred to as automatic balancing is used in Herzog et al, 1996; Lum et al, 1996; Mohamed & Busch-Vishniac, 1995. This strategy is not feasible in many applications, such as milling or grinding, due to the desired goal of rotating a shaft about its geometric center.

2.2 Modeling Magnetic Bearing Dynamics

A mathematical model of the bearing is required before a controller can be designed. There are many models developed in the literature from physical principles applied to the system. All of the models require some approximations, assumptions and linearization of the plant around its operating point. A model for a non-rotating but flexible shaft is developed in each of Magnetic Moments, 1997; Nonami & Yamaguchi, 1992; Suzuki, 1998; Tian & Nonami, 1996 while a rotating and rigid shaft is modeled in Charara et al, 1996; Mohamed & Busch-Vishniac, 1995; Rundell et al, 1996; Smith & Weldon, 1995. Lum et al, 1996 presents a model of a planar spinning rotor. Complete models of the flexible, rotating shaft are presented in Sivrioglu & Nonami, 1998 and using the dynamic theory of flight in Matsumura & Yoshimoto, 1986.

The method presented in Lee et al, 1995 uses closed loop data from a magnetic bearing excited with noise to estimate properties such as stiffness, damping and current stiffness of an open loop physical model. This method overcomes the difficulty of accurately measuring some features of the apparatus by using a physical model. The model will contain approximations leading to inaccuracies that cannot be overcome using this method. AMB systems often show discrepancies between the predicted and the measured dynamic behavior due to the inaccurate modeling associated with magnetic forces, frequency characteristics of power amplifiers and electromagnets, leakage and fringing effects of magnetic fluxes and eddy current effects (Lee et al, 1995).

Since the plant is open loop unstable it is impossible to record open loop data to identify a model. The problem of identifying a MIMO closed loop plant is difficult and

frequency methods such as in Li & Lee, 1996 rely on open and closed loop data. The open loop dynamics of a closed loop plant with known discrete feedback dynamics can be identified using the method provided in Phan & Longman, 1994. Using only SISO plant input and output data, a discrete model with the least squared error can be estimated using the method in Ljung, 1999 in either a recursive or a batch configuration. The least squares estimation method can be easily extended to a multiple input, single output identification. That is, models found from this type of identification are highly application specific.

The author was unable to find any published material that does not use a physical principles model to design a controller for a magnetic bearing. Therefore the techniques described in Chapter 4 showing experimentally based modeling represent a significant contribution to the literature.

2.3 Control Strategies for a Magnetic Bearing

A controller used to levitate the shaft must have some robustness or in other words be able to operate under varying conditions. The controller must be robust to modeling errors, disturbances, non-linearities and varying plant dynamics which are unavoidable in any control application. The desire for greater robustness has lead to increased interest in non-linear controllers with guaranteed robustness properties.

2.3.1 Analog controllers

Analog PID controllers were the first algorithms used to successfully levitate a shaft. The tuning of these controllers was sometimes done by trial and error and produced a va-

riety of closed loop dynamics (Humphris et al, 1986). There is a trade-off in the tuning between control saturation, system stiffness and prevention of bearing touchdown. Acceleration feedforward with a digital PID controller was shown to reduce the deviation of the shaft due to ground motion in Suzuki, 1998 reducing the required level of trade-off. In a complete design approach, Sheu et al, 1995 considers the PD feedback parameter tuning and magnetic bearing location as one optimization problem.

The SISO nature of PID controllers reduces its effectiveness in an interactive MIMO system and often has poor robustness. A sliding mode controller was shown to be very effective and superior to a PID controller in Nonami & Yamaguchi, 1992 and Tian & Nonami, 1996. The application of sliding mode control to a magnetic bearing is desirable since it is theoretically very robust to a class of system variations and disturbances.

2.3.2 Digital Controllers

The implementation of digital controllers for magnetic bearings is computationally intensive and can only be achieved on a fast PC or DSP. The fast dynamics of the magnetic bearing require a fast sampling rate and complex controllers must be executed every sample interval. For example, a sample rate of 5kHz was chosen for the work done in this thesis. Several different digital control strategies outlined below have been simulated and experimentally tested in the literature.

The following implementations have been detailed:

- Herzog et al, 1996 analysed the stability and inserted generalised notch filters in conjunction with the existing controller in an industrial turboexpander to achieve automatic balancing

- Automatic balancing was simulated using an on-line identification of physical characteristics of the imbalance to tune the stabilizing controller in Lum et al, 1996.

- Imbalance compensation and automatic balancing was simulated in Mohamed & Busch-Vishniac, 1995 using Q-parameterization theory.

- Simulations of an integrator backstepping controller for a planar rotor disk, magnetic bearing system was presented in Queiroz & Dawson, 1996.

- To achieve system robustness, H_∞ control strategy (Dahleh & Diaz-Bobillo, 1995) has been implemented to magnetic bearings. Using the loop shaping design procedure, a gain scheduled H_∞ controller for automatic balancing was simulated and experimentally tested in Matsumura et al, 1996.

- In Sivrioglu & Nonami, 1998 a gain-scheduled H_∞ controller was also implemented using the linear parameter varying (LPV) approach where the time-varying parameter is the rotational speed of the shaft. The LPV method has received some attention in other applications such as vehicle suspension (Fialho and Balas, 1998).

- The μ synthesis design method (Skogestad & Postlethwaite, 1996) was evaluated using simulations and experiments in Nonami & Ito, 1996. The results show a greater robustness to mass variation in the shaft than the H_∞ controllers but the synthesis requires a solution to an iterative and nonconvex numerical procedure.

- A fuzzy controller was designed in Vidolov et al, 1996 and the simulated results are comparable to a sliding mode controller.

2.3.3 Linear Quadratic Controllers

The optimal or linear quadratic (LQ) controller relies on linear state feedback to minimize a designed cost function made up of the states and the control action. The LQ controller has been applied to many systems and is a well documented control strategy (Anderson & Moore, 1990; Skogestad & Postlethwaite, 1996). An optimal integral-type controller for an AMB is implemented in Matsumura & Yoshimoto, 1986 including simulation and experimental results.

2.3.4 Sliding Mode Controllers

Sliding mode control (SMC) theoretically features excellent robustness properties in the face of parametric uncertainty (inaccuracies in the constants of a model and matched exogenous disturbances) making it an attractive controller for a magnetic bearing. The theory and design of continuous sliding mode controllers was well introduced and illustrated in DeCarlo et al, 1996; Slotine & Li, 1991; Utkin, 1977. A Discrete Sliding Mode Controller (DSMC) for a discrete plant was presented in Pieper & Surgenor, 1993 along with an application example showing DSMC robustness compared to an LQ controller and in Furuta, 1990. Pieper & Surgenor, 1993 also provided methods for calculating optimal sliding surfaces or constraining closed loop dynamics.

Simulated results of a SMC for a magnetic bearing were presented in Lewis et al, 1998, Smith & Weldon, 1995 and with a sliding mode observer for a vertical shaft in Rundell et al, 1996. Experimental results of a sliding mode controller were presented in Nonami & Yamaguchi, 1992 , Tian & Nonami, 1996 and in a test rig with no bias current in Charara et al, 1996. All of the sliding mode controllers found in the literature used a single sliding surface.

A discrete time version of the sliding mode control law was implemented in Tian & Nonami, 1996 with a different switching condition than in Pieper & Surgenor, 1993. All the other implementations use a continuous time sliding mode control law with a discrete implementation requiring a fast sampling rate. The SMC in Nonami & Yamaguchi, 1992 used a 4kHz sampling rate for a first critical frequency of 55Hz while in Sivrioglu & Nonami, 1998 a rate of 3.6kHz was used for the 100 Hz first critical frequency. The DSMC in Tian & Nonsami, 1996 sampled relatively slower at 5kHz for a first critical frequency of 340Hz. The apparatus used for the work in this thesis has a first critical frequency of about 800Hz (Magnetic Moments, 1997) and a relatively slow sampling rate of 5kHz was stable using the DSMC given in Pieper & Surgenor, 1993.

A combined digital DSMC and digital PI controller for a motor speed controller was presented in DeSantis, 1989 giving good disturbance rejection and tracking performance. These features are desirable for a magnetic bearing application.

DSMC is a good choice of controller for a magnetic bearing due to its robustness to uncertainty and disturbances shown in Pieper & Surgenor, 1993 and Furuta, 1990.

2.3.5 Observers

Many control algorithms rely on state information for feedback control. Models of magnetic bearings contain more states than outputs so an estimator is required to estimate the states from the available outputs. A Kalman filter provides a least squares state estimate from the outputs of the system for given noise and disturbance variances (see Anderson & Moore, 1990; Skogestad & Postlethwaite, 1996).

A sliding mode observer potentially offers advantages similar to those of sliding controllers, in particular inherent robustness to parametric uncertainty. The chattering in a sliding mode observer is just a numerical feature unlike the hard mechanical chattering in the sliding mode controller. The potential use of sliding observers was discussed in Slotine et al, 1987. A sliding observer was proposed in Walcott & Zak, 1987 with a numerically tractable solution to the observer design presented in Edwards and Spurgeon, 1994. The design example in Edwards and Spurgeon, 1994 was duplicated and compared to a Kalman filter for non-zero initial states. The Kalman filter was found to match the actual states more quickly than the sliding mode observer. The initial condition of a magnetic bearing when it is ready to lift off from its mechanical supports has non-zero states so based on this comparison a Kalman filter may perform better than a sliding mode observer. For this reason, a Kalman filter was chosen to estimate the states of the magnetic bearing.

2.4 Summary

In this chapter some applications for magnetic bearings along with their basic operation was discussed. The current state of research in controllers for magnetic bearings as well as some control strategy background was presented. It was noted in the review of the literature that only a physical analysis of a magnetic bearing has been used to produce a model even though there exists several experimental approaches to modeling.

Chapter 3
Apparatus

3.1 Introduction

In this chapter the magnetic bearing apparatus and the controller implementation hardware and software are described. The bearing apparatus is laboratory scale but is typical of industrial applications such as for natural gas compressor stations.

The proposed external controller implementation consists of a PC with an analog to digital (ADC) and digital to analog (DAC) conversion board. The software to run the control algorithm and the communication board is Matlab (Math Works, 1996) with the Simulink toolbox and the WinCon (Qanser Consulting, 1998) real time execution software package.

3.2 Magnetic Bearing Research Equipment

The magnetic bearing apparatus is a laboratory-scale system manufactured by Magnetic Moments (Magnetic Moments, 1997) shown in Figure 3.1. The system consists of a shaft 0.269m long weighing 0.262kg that can be levitated at both ends by electromagnets in both horizontal and vertical directions. When the shaft is levitated, it can be rotated by hand and spins without contact with the supporting structure.

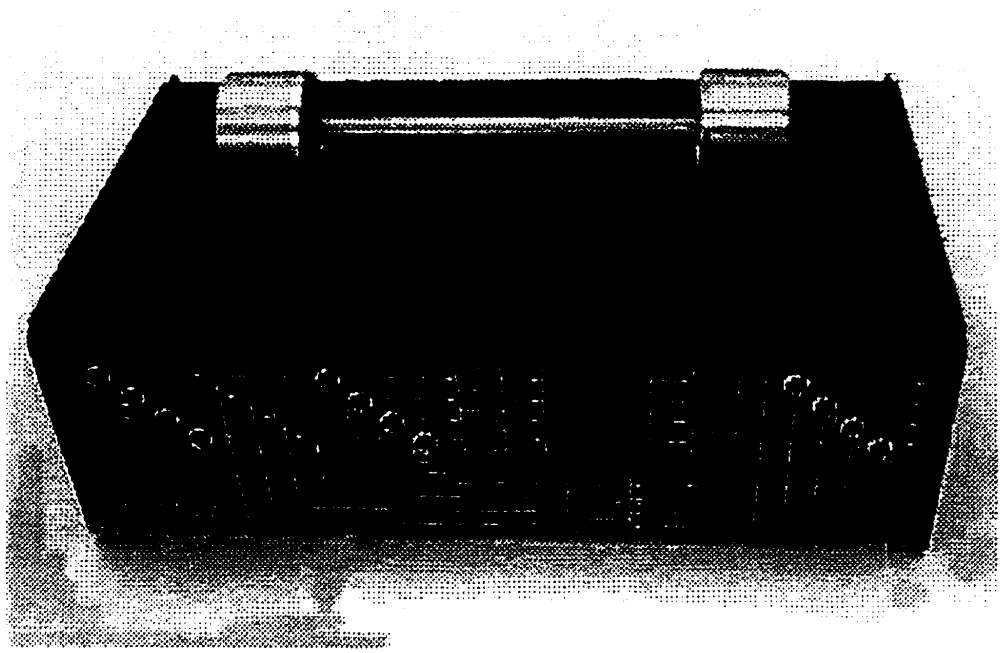

Figure 3.1 Magnetic Bearing Apparatus

The faceplate of the apparatus is shown in Figure 3.2. Through this faceplate, the following connections are available:

- Four outputs which provide position measurements (A). One horizontal and one vertical output at each end of the shaft at a nominal scale of 1Volt/0.1mm. The shaft touches the housing at a position measurement of about $\pm 2.3V$.
- Four outputs which provide a measurement of the input to the current amplifiers (B). The current amplifiers produce 0.25A/Volt.
- Four inputs which can be added to the compensator feedback (C).
- Four buttons which close the feedback loops of the built-in compensators (D).

- Built-in compensators (E) can be used if buttons (D) are closed. If buttons (D) are open external control can be effected by measuring (A) and applying control inputs to (C).

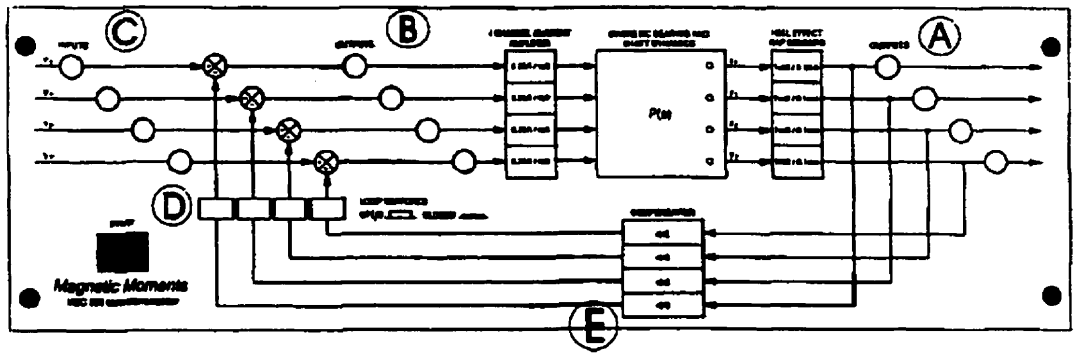

Figure 3.2 Magnetic Bearing Apparatus Faceplate (Magnetic Moments, 1997)

At each end of the shaft there are electromagnets to move the shaft in horizontal and vertical directions as well as position sensors for horizontal and vertical displacements located as in Figure 3.3. There are a pair of horseshoe-shaped electromagnets horizontally opposed and a pair vertically opposed with the same layout as in Figure 2.1 at each end of the shaft. The two magnets in each pair operate together by simultaneously increasing and decreasing the current about the bias current (or the nominal level).

Active control of the apparatus uses the four measured displacement signals to adjust the current in each of the electromagnet pairs. The four feedback compensators built-in to the apparatus are analog devices predesigned by the manufacturer with nominal dynamics (Magnetic Moments, 1997):

$$V(s)_{Control} = \frac{1.45\,(1 + 0.9 \times 10^{-3}s)}{(1 + 3.3 \times 10^{-4}s)\,(1 + 1.5 \times 10^{-5}s)} V(s)_{Sense} \qquad (3.1)$$

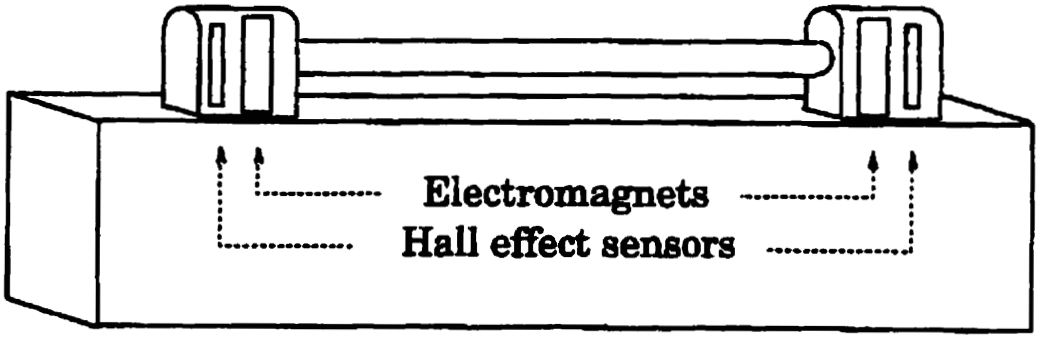

Figure 3.3 Active Magnetic Bearing Apparatus (Magnetic Moments, 1997)

3.3 Digital Controller Implementation

A schematic diagram of the control signal flow is shown in Figure 3.4. The four position outputs from the apparatus were connected to an ADC in a PC where they were sampled. The control algorithm was implemented in Simulink and the outputs from the controller were connected to the DAC and then to the apparatus inputs. The built-in compensators were disconnected using the push buttons on the front of the apparatus.

3.3.1 Hardware

The PC used to run the control algorithm was a Pentium II 350 with 96MB of RAM running Windows 95. The computational speed of this computer was the limiting factor in choosing the sample period of the controller. A faster sampling rate provides better

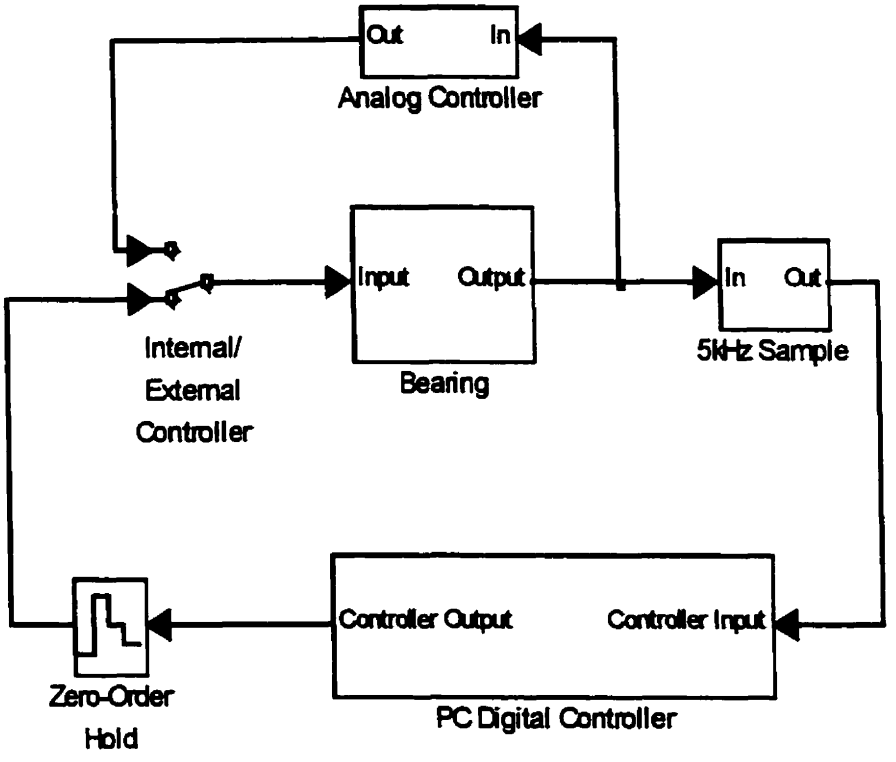

Figure 3.4 Digital Controller Signal Flow

resolution of the analog inputs and allows the controller to make control actions more often. The first critical frequency of the shaft is approximately 800Hz (Magnetic Moments, 1997) and a control systems rule of thumb states that the sampling should be at least five times faster than all frequencies of interest. A sampling rate of 5kHz was chosen to meet this rule with the first critical frequency while not exceeding the computational speed of the computer. This is a relatively slow sampling frequency compared to other applications (for example Nonami & Yamaguchi, 1992; Sivrioglu & Nonami, 1998).

The MultIQ I/O board from Quanser Consulting Inc was used to perform all of the data acquisition and analog outputs for the controllers. This board allows eight 13 bit bipolar analog inputs in the range of $\pm 5V$ along with eight 12 bit analog outputs in the range of $\pm 5V$. From the analog frequency measurements in Section 4.3 it was found that the analog output signals were very small above 2.5kHz so with the sample rate chosen to be 5kHz, anti-aliasing filters were unnecessary.

3.3.2 Software

The Matlab/Simulink v5.2 software package (Math Works, 1996) was used to design and implement all of the digital controllers. Matlab provided all of the mathematical calculations and Simulink was used to connect the control signal flow to the I/O board using the Quanser Consulting Inc (Qanser Consulting, 1998) I/O Simulink blocks. The Simulink controller diagram was compiled to an executable using WinCon 3.0 to speed up the computations. The controllers were run using the WinCon interface which enabled graphing and data logging.

3.4 Summary

This chapter described the magnetic bearing apparatus and the equipment that was used to implement and test the digital controllers. The shaft of the laboratory scale magnetic bearing apparatus was levitated by the built-in analog compensators and by digital controllers implemented in Matlab, Simulink and WinCon on a PC.

Chapter 4
System Identification

4.1 Introduction

In this chapter the details of the procedure and results of modeling the magnetic bearing are presented. To implement a control strategy for any plant it is essential to have a model. The large majority of control strategies require a linear model. This model must be sufficiently accurate so that controllers designed based on the model will result in a closed loop system which meets the control objectives. The main objective of the magnetic bearing controller is to be able to levitate the shaft from its supports and maintain this levitation in the presence of all reasonable disturbances. This chapter discusses the three methods that were used to try and produce a model that was accurate enough to be used as a basis for designing a stable controller for the magnetic bearing apparatus.

4.2 Physical Analysis

A linear two input (u_{hl} and u_{hr}), two output (y_{hl} and y_{hr}) model of the magnetic bearing horizontal dynamics was made using the outline in Magnetic Moments, 1997 which took into account the physics of the major components of the system. The same model can be used for the vertical dynamics (u_{vl}, u_{vr}, y_{vl} and y_{vr}) since the apparatus is constructed symmetrically. This approach uses Newtons Laws of motion. The operating point of the system under closed loop should be horizontally and vertically centered at each end of the

shaft. The model was calculated using small deviation linear approximations around this point. This model did not take into account any dynamics related to a rotating shaft but did include:

- The rigid shaft properties as well as the flexible dynamics.
- A linear approximation of the force on the shaft exerted by the current in the coils of the electromagnets.
- The dynamics of the current amplifier that regulate the current to the coils.
- A linear approximation of the displacement sensors.

The poles of the analytical model are shown in Figure 4.1 with the frequency response shown in Figure 4.2. The frequency response uses mirror image maps of the unstable poles with an appropriate phase shift to generate the response. The system is symmetric so that the response of y_{hl}/u_{hr} is the same as y_{hr}/u_{hl} and y_{hr}/u_{hr} is the same as y_{hl}/u_{hl} and the vertical axes responds similarly so this model can be extended to a four input, four output model of the whole plant assuming that there is no coupling between the axes.

The right half poles in Figure 4.1 show that, as expected, the plant is unstable. It also shows that there are two lightly damped resonant modes at 780Hz and 2,150Hz which can also be seen by the sharp peaks in Figure 4.2.

This model was used to design an LQG controller for the horizontal axis with the built-in compensators maintaining the vertical position. It was not possible to produce a closed loop stable system with this LQG controller. Many different controller and observer

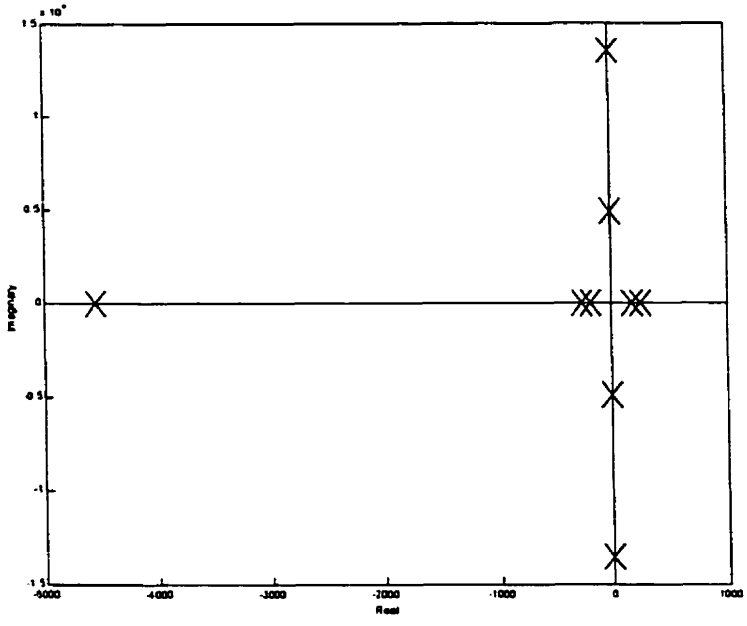

Figure 4.1 Open Loop Poles of the Analytical Model of One Axis

tuning choices were made and in the end the instabilities were attributed to modelling inaccuracies.

4.3 Frequency Response Analysis

4.3.1 Closed Loop Frequency Response

This method of producing a model of the plant involved adding a sine wave to one of the inputs then measuring the relative amplitude and relative phase of each of the outputs. These measurements were done using analog instruments and were recorded using the ADC. The frequency was swept over a range and the result was the linear approximation of

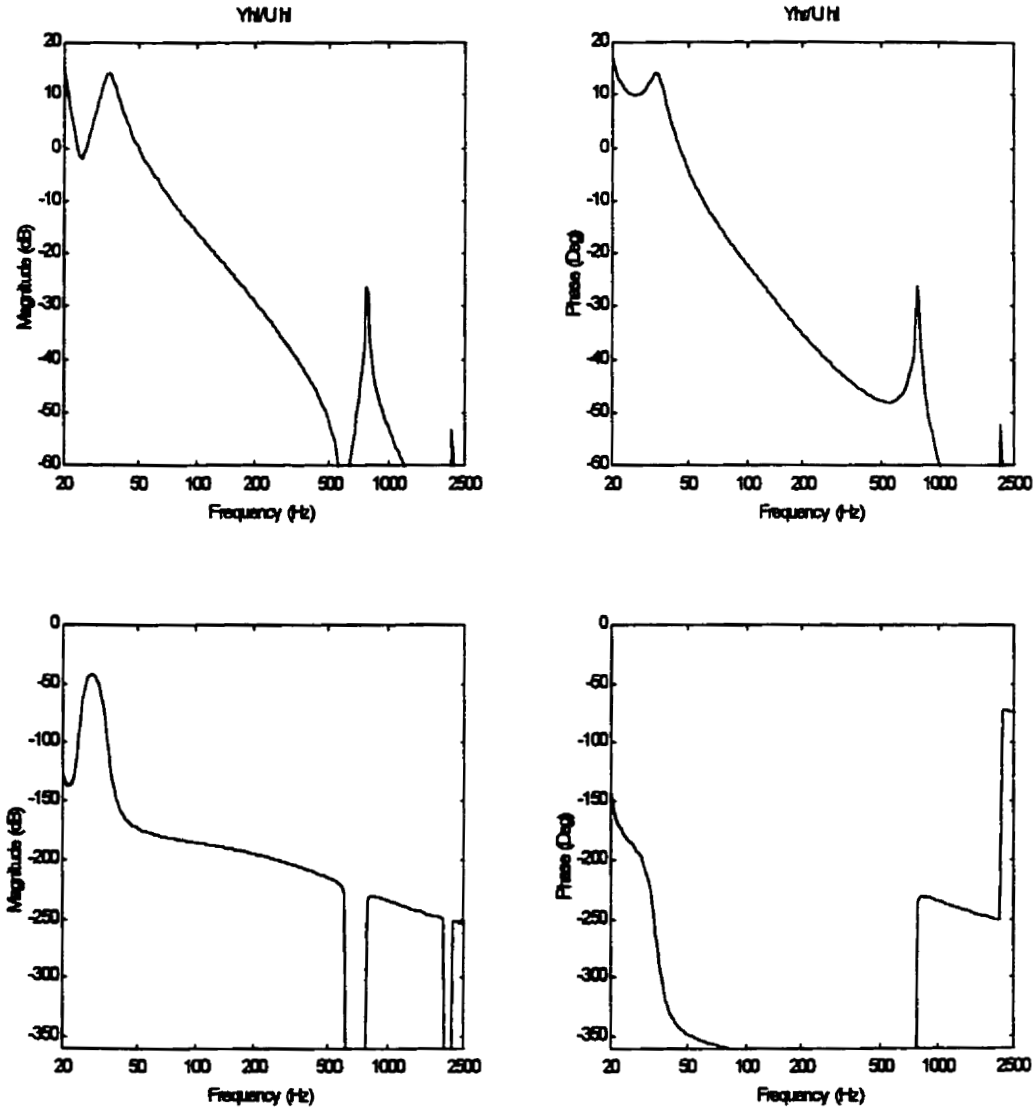

Figure 4.2 Frequency Response of Open Loop Analytical Model of One Input to Outputs on Same Axis

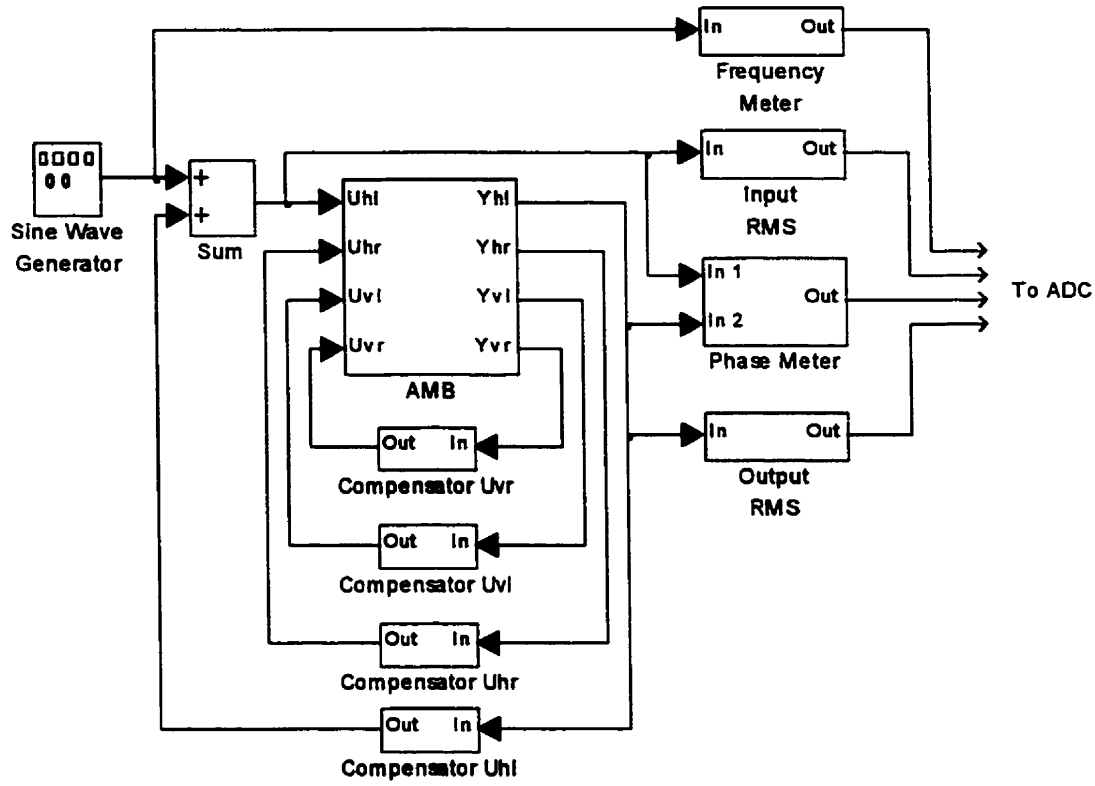

Figure 4.3 Closed Loop Frequency Response Measurement Connections for U_{hl} Input

the frequency response of the closed loop system from each input to each output. The low frequency limit of 20Hz was caused by the range of the available amplitude RMS meters and the upper limit of the range was chosen to be close to the Nyquist frequency of the digital controller to be implemented. The measured signals are shown in Figure 4.3.

The measured output was not a pure sine wave and contained some other frequencies indicating that the plant is not linear. The measured frequency response of the horizontal outputs to u_{hl} are shown in Figure 4.4. There is a strong resonance at 780Hz which is the same as the analytical model in Section 4.2 although the resonance at 2,150Hz was

not observed. There was negligible coupling between the two axes and the response was virtually identical from the left or right ends except for a small gain difference. The vertical axis was also found to be almost identical to the horizontal axis. The resonant peak is very sharp indicating that it is very lightly damped. Measurement noise limited the magnitude data to a minimum of -40dB.

4.3.2 Model Synthesis from Frequency Response Data

A transfer function was fitted to the frequency response data. Figure 4.5 shows the frequency response of the transfer functions as well as the data it was designed to match. The magnitude and phase match very closely. These transfer functions were fitted using the 'fitsys' and 'magfit' Matlab commands which uses a least squares fitting criteria and required careful choice of the fitting weighting function as well as manual placement of some of the poles into the right half plane to match the measured phase response. The y_{hl}/u_{hl} model was a sixth order transfer function and the y_{hr}/u_{hl} model was fourth order.

4.3.3 Modeling Results

Using the two transfer functions shown in Figure 4.5 and assuming that the plant is symmetrical in both the left to right and horizontal to vertical comparisons, then it is mathematically possible to determine the open loop plant from these closed loop models if the built-in compensator dynamics are accurately known. In practice, this was numerically difficult and heavily sensitive to variations in some of the transfer function coefficients. Also, the built-in compensator dynamics from equation 5.22 are not accurately known since each

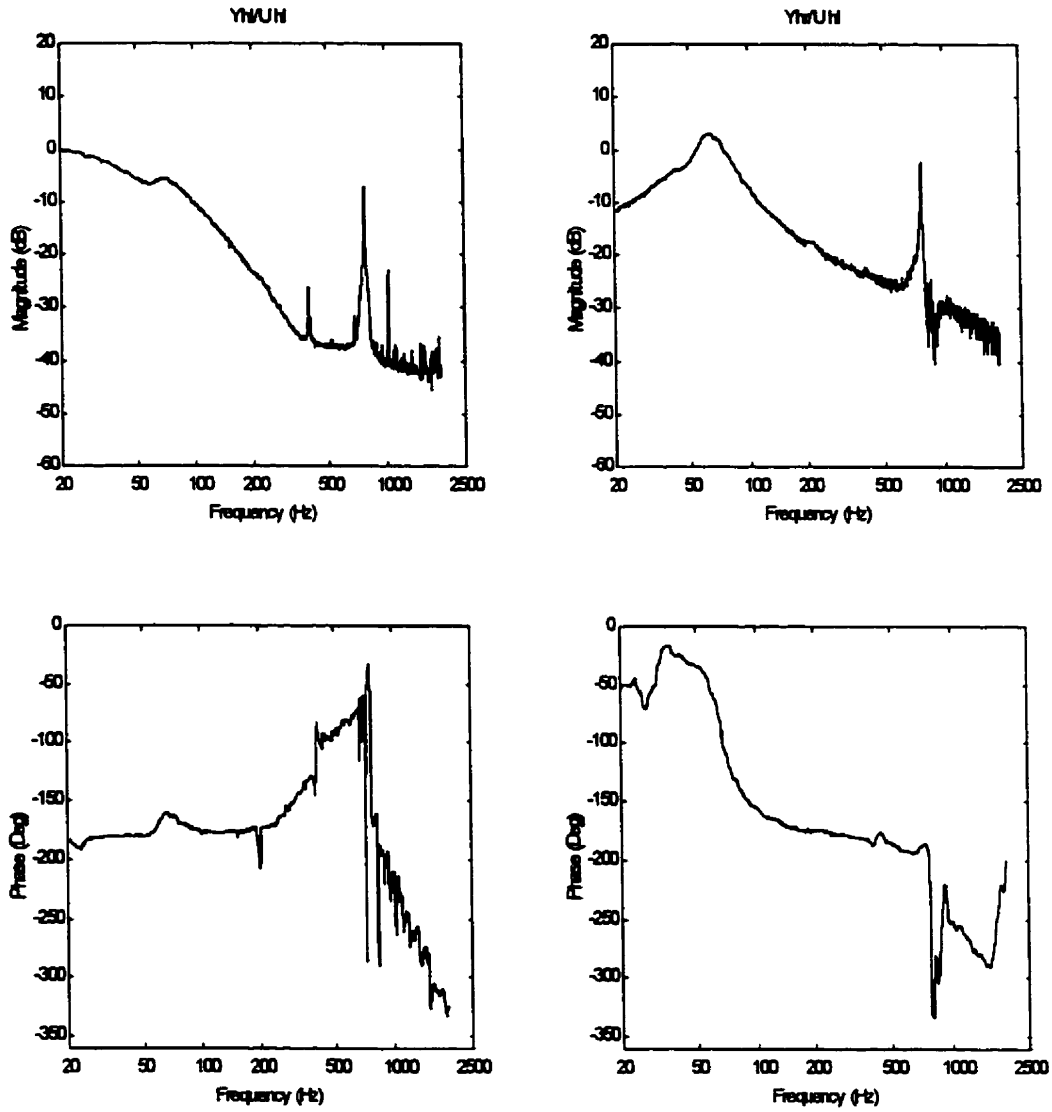

Figure 4.4 Measured Frequency Response of Horizontal Axis to Left Horizontal Input with Built-In Compensator Feedback.

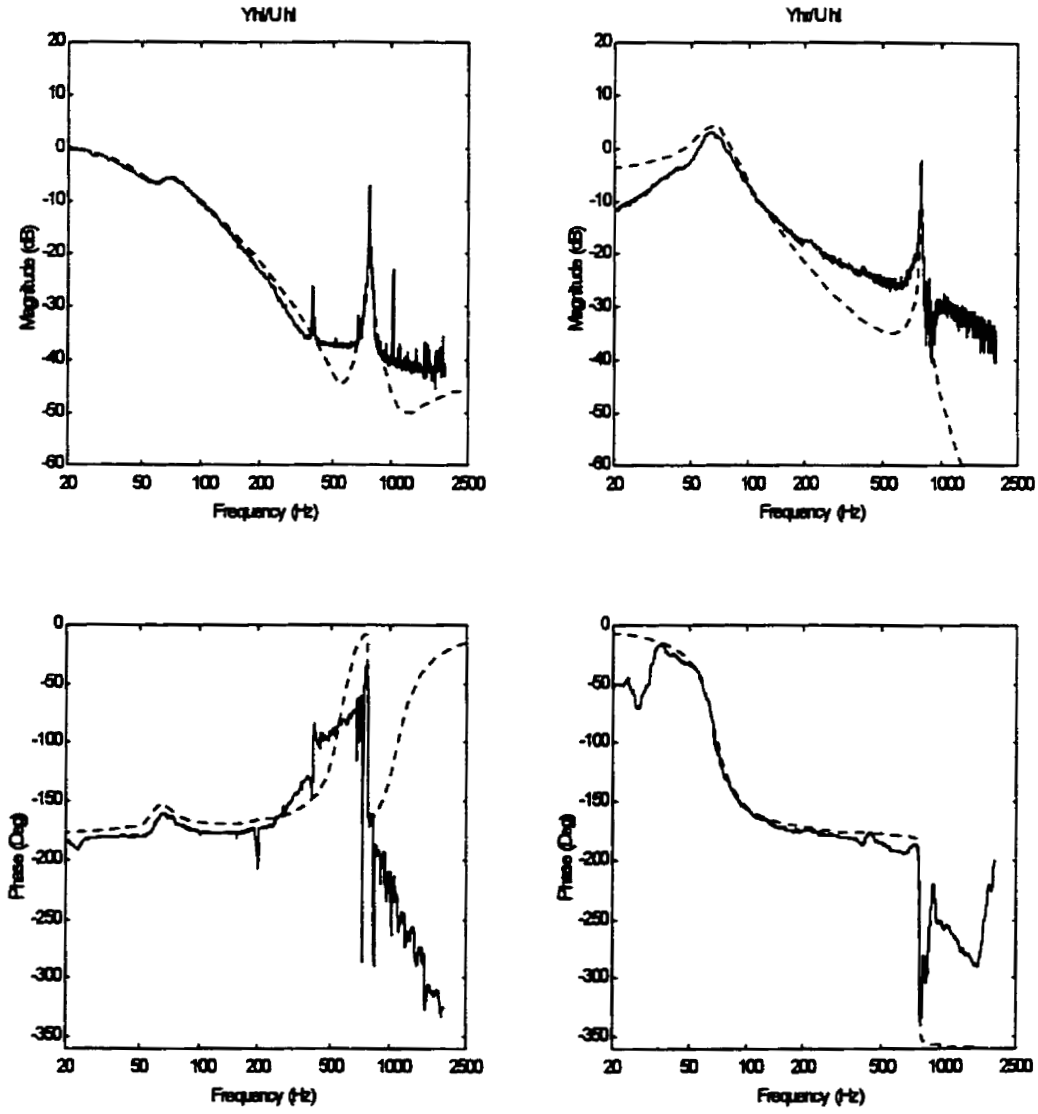

Figure 4.5 Frequency Response of Horizontal Axis Model to Left Horizontal Input with Built-In Compensator Feedback. (Model:···, Data:—)

compensator was individually tuned by the manufacturer. The dynamics of the compensators could not be measured without dismantling the apparatus. This method of identification yielded no useful plant model since the solution is parametric in the controller. If the controller was known then this method could be useful in identifying the plant.

4.4 Parameter Estimation

Parameter estimation was used to identify the coefficients of difference equations to model the plant. This method of identifying a discrete model uses input and output data and produces a least squares estimate of the plant parameters. The order of the plant must be specified as must the pure delay from the input to the output.

4.4.1 Least Squares Batch Parameter Estimation Method

The following algorithm for batch parameter estimation is from Ljung, 1999 with an extra input added to the equations. The plant is modeled by Equation 4.2.

$$A\left(q^{-1}\right) y_k = q^{-d} B_1\left(q^{-1}\right) u_{1,k} + q^{-d} B_2\left(q^{-1}\right) u_{2,k} + w_k \tag{4.2}$$

where:

$u_{1,k}$ and $u_{2,k}$ are the inputs at time step k

y_k is the output at time step k

w_k is white Gaussian noise at time step k

d is the number of time steps of pure delay

q^{-1} is the unit delay operator

$$A(q^{-1}) = 1 + a_1 q^{-1} + \cdots + a_n q^{-n}$$

$$B_1(q^{-1}) = b_{10} + b_{11} q^{-1} + \cdots + b_{1m} q^{-m}$$

$$B_2(q^{-1}) = b_{20} + b_{21} q^{-1} + \cdots + b_{2m} q^{-m}$$

n is the order of the output difference equation

m is the order of the input difference equations

and $m \leq n$

Equation 4.2 can be rewritten in matrix form as:

$$y_k = \begin{bmatrix} -a_1 & \cdots & -a_n & b_{10} & \cdots & b_{1m} & b_{20} & \cdots & b_{2m} \end{bmatrix} \begin{bmatrix} y_{k-1} \\ \vdots \\ y_{k-n} \\ u_{1,k-d} \\ \vdots \\ u_{1,k-d-m} \\ u_{2,k-d} \\ \vdots \\ u_{2,k-d-m} \end{bmatrix} + w_k \quad (4.3)$$

$$y_k = \phi_k^T \theta + w_k \quad (4.4)$$

where:

$$\theta^T = \begin{bmatrix} -a_1 & \cdots & -a_n & b_{10} & \cdots & b_{1m} & b_{20} & \cdots & b_{2m} \end{bmatrix} \quad (4.5)$$

$$\phi_k^T = \begin{bmatrix} y_{k-1} & \cdots & y_{k-n} & u_{1,k-d} & \cdots & u_{1,k-d-m} & u_{2,k-d} & \cdots & u_{2,k-d-m} \end{bmatrix} \quad (4.6)$$

Let

$$Y = \begin{bmatrix} y_1 & \cdots & y_{kmax} \end{bmatrix}^T \quad (4.7)$$

$$\Phi = \begin{bmatrix} \phi_1^T & \cdots & \phi_{kmax}^T \end{bmatrix}^T \quad (4.8)$$

where $k = 1, ..., k_{\max}$ is the time interval. The least squares estimate of θ is given by (Ljung, 1999):

$$\hat{\theta}(k) = \left(\Phi^T \Phi\right)^{-1} \Phi^T Y \tag{4.9}$$

4.4.2 Modeling Results

Noise was added to an input while the shaft was levitated using the built-in compensators. The noise source was a white noise generator along with a sine wave at the same frequency as the first resonant mode of the plant (as found by the measurements in Section 4.3). The noise was produced by a Simulink program at a 5kHz rate and the two outputs on the same axis as where the noise was added were recorded at the same sample rate. The test was repeated at the other end of the same axis and on each end of the other axis. The data was collected for about five seconds and a window of the data was used for the model identification after removing the D.C. component. The horizontal and the vertical model identifications followed the same method and had almost identical results. In each case, a two input, two output model was produced. For brevity, only the horizontal model is discussed. Equation 4.9 was used to identify 2 sub-systems:

$$A_1\left(q^{-1}\right) y_{hl} = q^{-d} B_1\left(q^{-1}\right) u_{hl} + q^{-d} B_2\left(q^{-1}\right) u_{hr} \tag{4.10}$$

$$A_2\left(q^{-1}\right) y_{hr} = q^{-d} B_3\left(q^{-1}\right) u_{hl} + q^{-d} B_4\left(q^{-1}\right) u_{hr} \tag{4.11}$$

The estimation was performed with $n = 8$, $m = 7$, $d = 1$, and $k_{\max} = 6000$. The choice of the plant order, n, was very important since low values of n gave large variations in the frequency response of the identified plant. Further increases in the value of n beyond

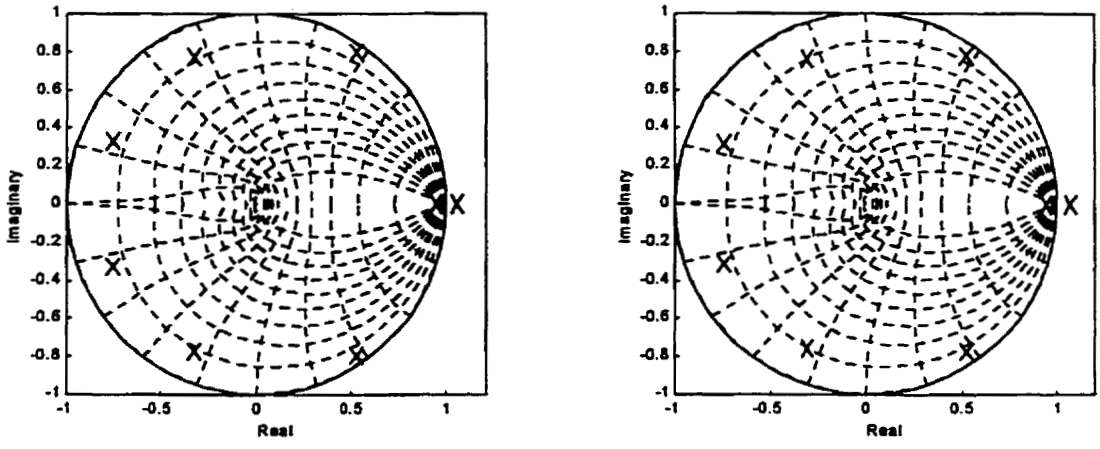

Figure 4.6 Poles of Horizontal Subsystems Identified Through Parameter Estimation. (Left: Roots of $A_1(q^{-1})$. Right: Roots of $A_2(q^{-1})$)

eight had little effect on the identified plant. The amount of data used in the identification algorithm, k_{max}, also had a large effect on the outcome of the identification but increasing values of k_{max} appeared to converge towards one model. The other two parameters, time delay d and the order of the input equations m, did not impact the modeling results significantly so were set to match the order of the output equation.

The poles of the identified subsystems given by the roots of the identified polynomials $A_1(q^{-1})$ and $A_2(q^{-1})$ were found to be almost identical as shown in Figure 4.6. This is consistent with the previous identification methods in Sections 4.2 and 4.3 and is to be expected since the apparatus was constructed symmetrically.

The roots of $A_1(q^{-1})$ and $A_2(q^{-1})$ were arithmetically averaged to produce a polynomial $A_3(q^{-1})$ so that equations 4.10 and 4.11 could be rewritten as equations 4.12 and 4.13.

$$A_3\left(q^{-1}\right) y_{hl} = q^{-1}\left(B_1\left(q^{-1}\right) u_{hl} + B_2\left(q^{-1}\right) u_{hr}\right) \quad (4.12)$$

$$A_3\left(q^{-1}\right) y_{hr} = q^{-1}\left(B_3\left(q^{-1}\right) u_{hl} + B_4\left(q^{-1}\right) u_{hr}\right) \quad (4.13)$$

This pair of two input, one output equations can be combined and rewritten in state space form as two sets of one input, two output systems:

$$x_{hl,k+1} = A_{hl} x_{hl,k} + B_{hl} u_{hl,k} \quad (4.14)$$

$$y_{h,k} = H_{hl} x_{hl,k} \quad (4.15)$$

$$x_{hr,k+1} = A_{hr} x_{hr,k} + B_{hr} u_{hr,k} \quad (4.16)$$

$$y_{h,k} = H_{hr} x_{hr,k} \quad (4.17)$$

where (see Appendix A):

$x_{hl,k}$ are the states of the left subsystem at time step k

$x_{hr,k}$ are the states of the right subsystem at time step k

$u_{hl,k}$ is the left horizontal input at time step k

$u_{hr,k}$ is the right horizontal input at time step k

$y_{h,k} = \begin{bmatrix} y_{hl,k} \\ y_{hr,k} \end{bmatrix}$ are the outputs at time step k.

A_{hl} and A_{hr} are 8x8 matrices

B_{hl} and B_{hr} are 8x1 matrices

H_{hl} and H_{hr} are 2x8 matrices

The two systems can be combined to give the two input, two output system

$$x_{h,k+1} = \begin{bmatrix} A_{hl} & 0_{8\times8} \\ 0_{8\times8} & A_{hr} \end{bmatrix} x_{h,k} + \begin{bmatrix} B_{hl} & 0_{8\times1} \\ 0_{8\times1} & B_{hr} \end{bmatrix} u_{h,k} \quad (4.18)$$

$$y_{h,k} = \begin{bmatrix} H_{hl} & H_{hr} \end{bmatrix} x_{h,k} \quad (4.19)$$

where:

$$x_{h,k} = \begin{bmatrix} x_{hl,k} \\ x_{hr,k} \end{bmatrix}$$

$$\text{and } u_{h,k} = \begin{bmatrix} u_{hl,k} \\ u_{hr,k} \end{bmatrix}$$

Equations 4.18 and 4.19 are the final identified horizontal model which has two inputs, two outputs and 16 states and was verified as completely controllable and observable. It can be rewritten as:

$$x_{h,k+1} = \Phi_h x_{h,k} + \Gamma_h u_{h,k} \tag{4.20}$$

$$y_{h,k} = H_h x_{h,k} \tag{4.21}$$

Figure 4.7 shows the frequency response of the horizontal model to the left horizontal input with a resonance at 782Hz. The phase response is quite different from the analytical model in Figure 4.2 but the magnitude shape is similar with a sharp resonance at 780Hz. The discrete poles in Figure 4.6 map quite closely after conversion to the continuous time poles of the analytical model in Figure 4.1 up to about 1kHz.

The parameter estimation method of identifying a model for a magnetic bearing produced good results. This method of system identification was not used in any published literature for a magnetic bearing.

4.5 Model Resonant Mode Refinement

A stable controller was built based on the parameter estimated model but the shaft resonated at the first resonant mode with all of the controller tunings tested. The resonant peaks are more heavily damped than the closed loop measurements which can be seen by

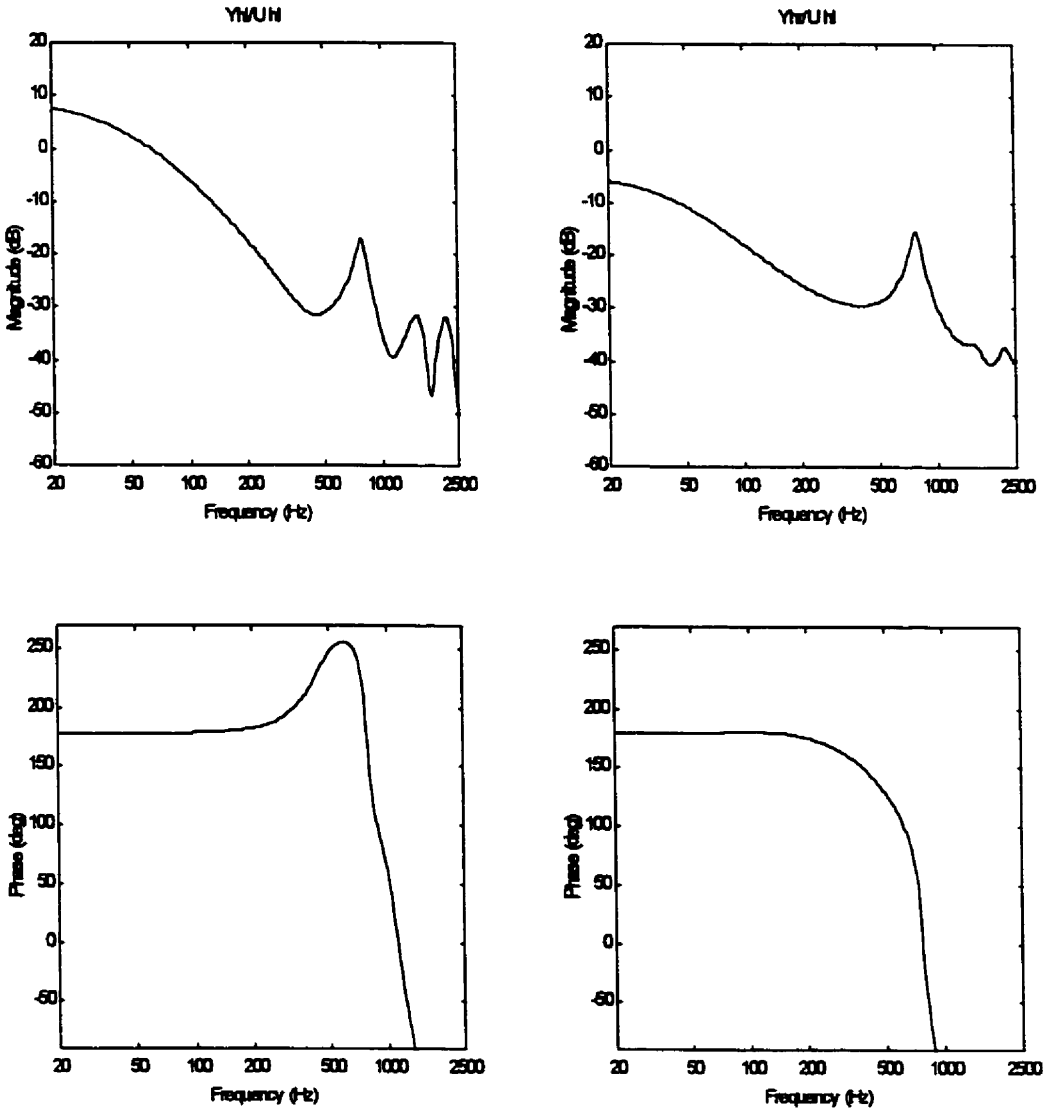

Figure 4.7 Frequency Response of Open Loop Horizontal Parameter Estimation Model to Left Horizontal Input

comparing Figure 4.7 with a resonant peak of about 15dB to Figure 4.4 with a peak of about 35dB at a frequency of 780Hz.

4.5.1 Model Refinement

The model was modified by moving the resonant poles closer to the unit circle (from a radial distance of 0.945 to 0.996) to decrease the effective damping in the resonance while maintaining the resonant frequency. The modified frequency response for the left horizontal input is shown in Figure 4.8 along with the original response. A controller design based on this model was stable and did not resonate.

The model with the relocated poles has a DC gain that is about 5% lower than the original model but this error is small and compensated for by the feedback controllers. The simulation in the following section was designed to shed some light on the performance of the parameter estimation method for a resonant pole.

There will be some bias in the estimation since the plant input noise is coloured rather than a white noise source (Ljung, 1999) which could account for the error in the model identification. The colouring of the plant input noise comes from the addition of the external excitation noise to the compensator feedback to produce the plant input.

4.5.2 Simulation of System Resonant Mode Identification

A numerical simulation was performed to investigate the identification of a linear plant with a resonant peak. Discrete white noise (in the range of ± 1 at 5kHz) with a sine wave (amplitude 1) at the resonant frequency was used as input to a continuous transfer

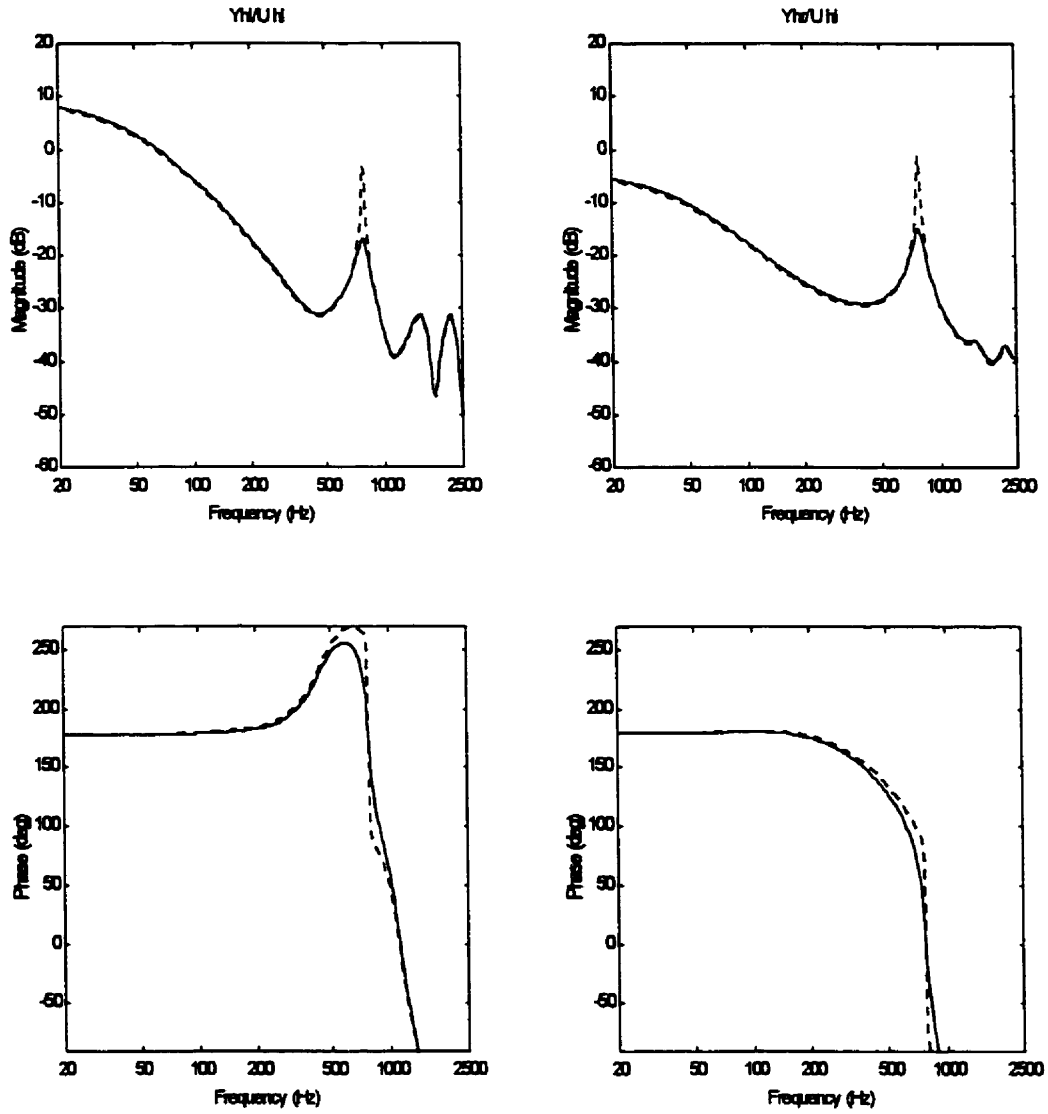

Figure 4.8 Frequency Response of the Open Loop Modified Parameter Estimation Model Horizontal Outputs to the Left Horizontal Input (Original Model (-), Modified Resonance (- - -))

function with a resonance at 800Hz and damping of about 0.004 (similar to the final parameter estimation model). The output data was recorded and the plant was identified using the parameter estimation method and then Gaussian noise (mean: 0, variance: 0.05) was added to the output and the identification procedure was repeated. Figure 4.9 shows the frequency response of the original plant and the two identification results. It is clear from this simulation that with noise in the measurement, the ability to identify this resonant peak is reduced (peak of 5dB compared to 40dB).

Figure 4.9 shows that the DC gain of the identified model with noise in the measurement is significantly higher than the model identified without noise. From this brief simulation it appears that the identified model with a higher damping is accompanied with a higher DC gain and for this reason the DC gain of the magnetic bearing model with modified resonant pole was not adjusted.

4.6 Summary

This chapter presented the attempted methods to model the magnetic bearing system. The physical analysis model was not accurate enough in this case to be used as a basis to design a stable controller. The sine wave response of the closed loop system with built-in compensators was measured then transfer functions were matched to the response. It was not possible to calculate an open loop model from this data due to numerical difficulties and inaccurate knowledge of the built-in compensators.

An open loop model was identified using the discrete parameter estimation method to identify subsystems from closed loop input/output data. The subsystems were then com-

bined to produce a two input, two output, 16 state open loop model for each of the horizontal and vertical axes. The models are open loop unstable and have a resonance at 782Hz. The resonance of the model was found to be too heavily damped to be used as a basis to design a controller so the resonant poles were modified to be more lightly damped. A numerical simulation was performed to investigate the misidentification of a sharp resonant peak with a noise corrupted measurement.

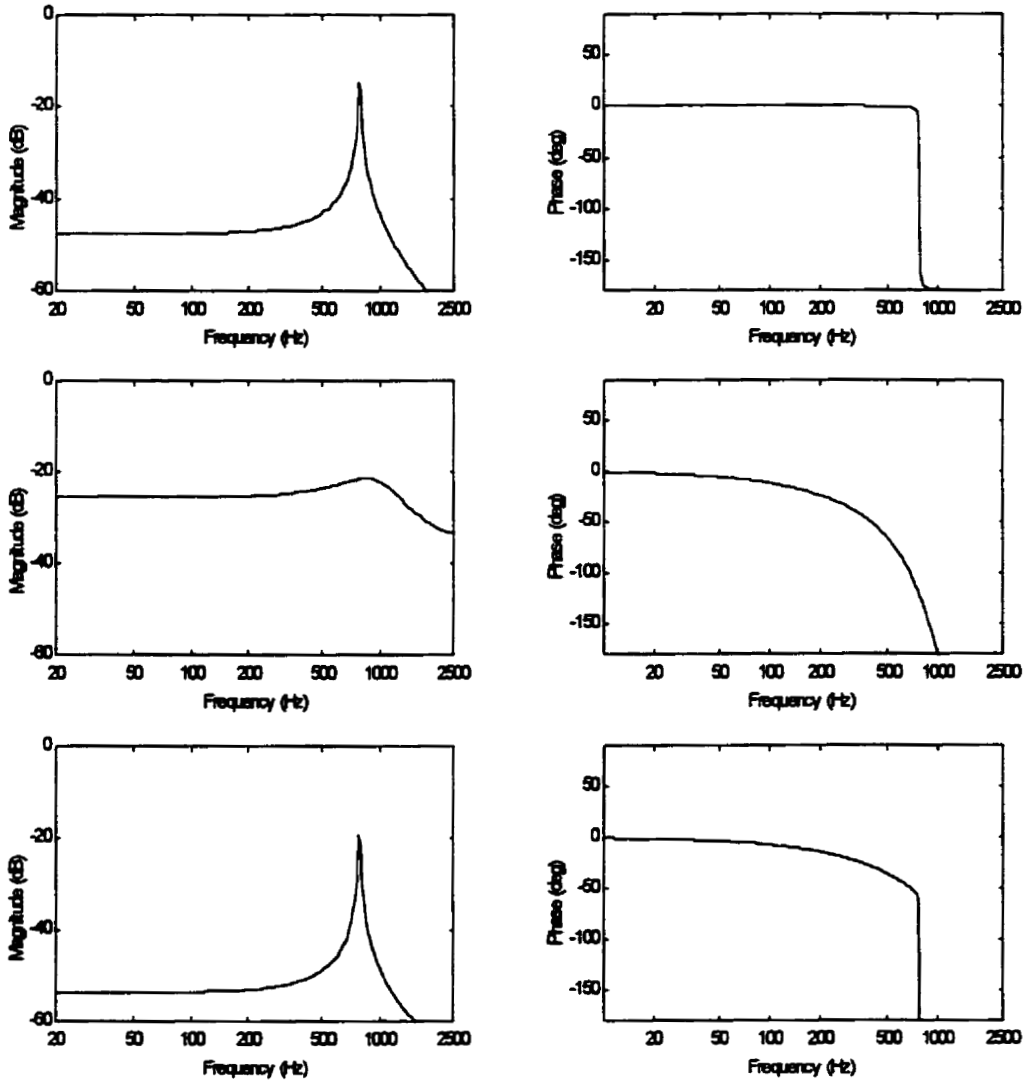

Figure 4.9 Frequency Response of Parameter Estimation Identification of a System with Sharp Resonance (Top) with Noise in the Measurement (Middle) and No Noise in the Measurement (Bottom)

Chapter 5
Control Law Development and Implementation

5.1 Introduction

In this chapter, details of the design and implementation of controllers for the magnetic bearing apparatus are presented. Firstly, the built-in compensators of the apparatus are discussed then several digital controllers are designed. The digital controller design is centered around the model identified in Section 4.4 and uses the equipment described in Chapter 3. Each digital controller consists of a separate horizontal and vertical component.

A state estimator for each axis was designed and state feedback controllers were implemented using the state estimates. An LQG controller was designed based on a selected cost function for each of the two axes. A modification to the plant model was made so that a DSMC could be implemented. The sliding surface for the DSMC was designed using a cost function to weight the control action and the output regulation objectives. An outer loop PI controller was added to the DSMC to improve its reference tracking ability. The DSMC was also modified to slide on different surfaces depending on the position of the ends of the shaft.

This chapter discusses the different controller tunings that were found to be stable as well as some tuning difficulties. The test results of these controllers and as well as the built-in compensators are detailed in Chapter 6.

5.2 Built-In Feedback Compensators

The magnetic bearing apparatus contains built-in feedback compensators as discussed in Section 3.2 which can be used to levitate the shaft. There are four single input, single output compensators which all use a position measurement and adjust the corresponding current in the electromagnet. There is reasonably strong coupling from one end of the shaft to the other on each axis of the shaft as seen in the identified model in Section 4.4. This means that there is significant dynamic coupling between the two control loops on each axis. With the single input, single output controllers there will be some interaction and possibly fighting between controllers on each axis which could result in oscillations in the closed loop dynamics.

The nominal compensator dynamics for each channel are given in Magnetic Moments, 1997 as:

$$V(s)_{control} = \frac{1.45\,(1 + 0.9 \times 10^{-3}s)}{(1 + 3.3 \times 10^{-4}s)\,(1 + 1.5 \times 10^{-5}s)} V(s)_{sense} \tag{5.22}$$

This has a frequency response shown in Figure 5.1.

5.3 Observer Design

An observer is required to estimate the states of the models identified in Section 4.4 for the LQ controller and DSMC to be implemented. For each of the axes, an observer is required that uses the two plant inputs and the two plant outputs to estimate the 16 states of the model. A Kalman filter was designed using the 'kalman' Matlab function (see

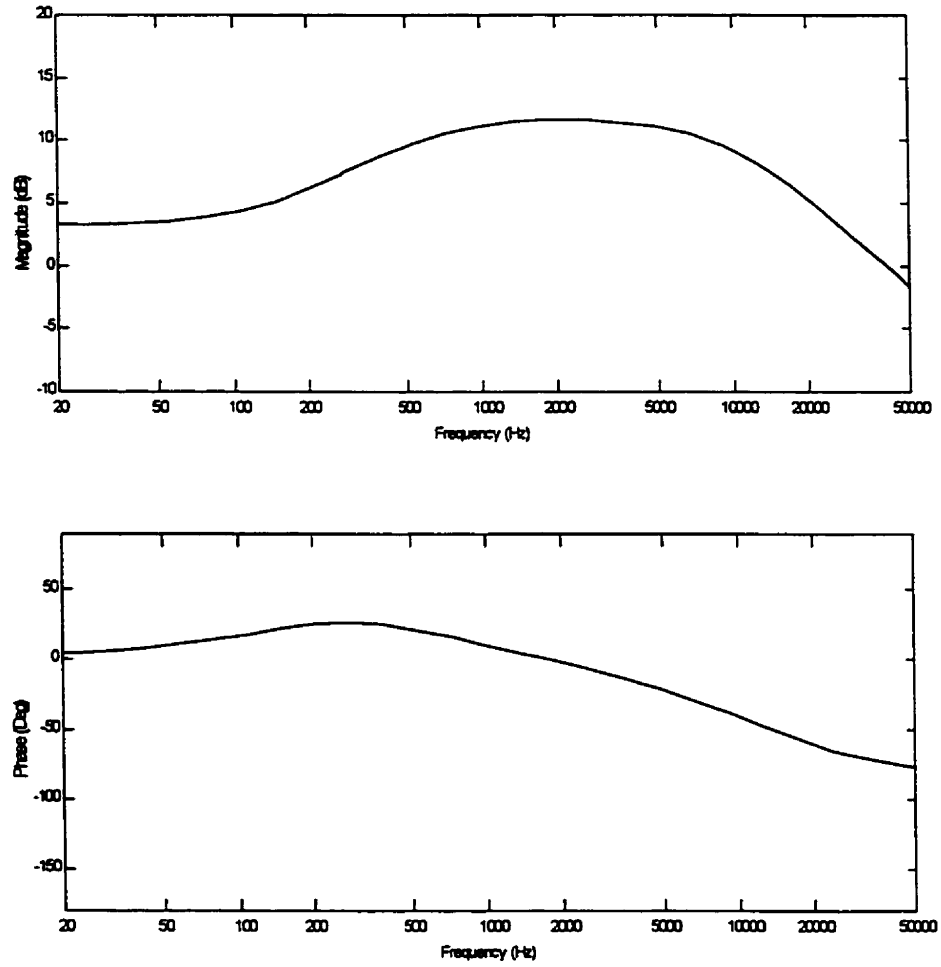

Figure 5.1 Built-In Compensator Nominal Frequency Response

Math Works, 1996). The structure of the horizontal system with matched white state noise (w) and measurement noise (v) is given by:

$$x_{h,k+1} = \Phi_h x_{h,k} + \Gamma_h \left(u_{h,k} + w_{h,k}\right) \tag{5.23}$$

$$y_{h,k} = H_h x_{h,k} + v_{h,k} \tag{5.24}$$

Where:

$$E\left[w_{h,k} w_{h,j}^T\right] = \begin{cases} Q_n & k = j \\ 0_2 & Otherwise \end{cases}$$

$$E\left[v_{h,k} v_{h,j}^T\right] = \begin{cases} R_n & k = j \\ 0_2 & Otherwise \end{cases}$$

$$E\left[w_{h,j} v_{h,k}^T\right] = 0_2 \qquad \forall k, j$$

$$E\left[w_{h,k}\right] = 0_2 \qquad \forall k$$

$$E\left[v_{h,k}\right] = 0_2 \qquad \forall k$$

Q_n, R_n Diagonal (i.e. the elements of w_h and v_h are independent.

The estimator that minimizes the steady-state error covariance:

$$P = \lim_{k \to \infty} E\left[\left(x_k - \hat{x}_k\right)\left(x_k - \hat{x}_k\right)^T\right] \tag{5.25}$$

is given by:

$$\hat{x}_{h,k+1} = \Phi_h \hat{x}_{h,k} + \Gamma_h u_{h,k} + L\left(y_{h,k} - H_h \hat{x}_{h,k}\right) \tag{5.26}$$

Q_n and R_n were roughly estimated to be $0.001 \times I_2$ from collected data while under closed loop control by the built-in compensators.

The 'kalman' Matlab function returns a state space system with four inputs (the two plant outputs and the two plant inputs), two filtered plant outputs and16 state estimates.

The estimator produces a least squares estimate of the states and the plant outputs without noise.

5.4 Linear Quadratic Gaussian Controller

5.4.1 Controller Synthesis

Two LQG controllers (one for the horizontal axis and one for the vertical axis) were designed using the identified models from Section 4.4 and the observer designed in Section 5.3. The controller was designed using the 'dlqr' Matlab function then combined with the observer using the 'lqgreg' function (Math Works, 1996). The control for the horizontal axis is $u_{h,k} = K_h \hat{x}_{h,k}$ which acts on the plant in equations 5.23 and 5.24. The 'dlqr' function calculates the optimal gain matrix, K_h (2×16), that minimizes a cost function, J, given by:

$$J = \sum_{k=0}^{\infty} x_{h,k}^T Q x_{h,k} + u_{h,k}^T R u_{h,k} \tag{5.27}$$

The matrix Q weights the deviation in the states while the R matrix provides the relative control action weighting. The cost function should reflect the goal of regulating the position of the shaft rather than directly regulating the states of the model which have no physical interpretation. The cost function was chosen to be:

$$J = \sum_{k=0}^{\infty} q y_{h,k}^T y_{h,k} + u_{h,k}^T u_{h,k} = \sum_{k=0}^{\infty} q x_{h,k}^T H_h^T H_h x_{h,k} + u_{h,k}^T u_{h,k} \tag{5.28}$$

So $Q = qH_h^T H_h$ and $R = I$. The design parameter, q, determines the relative weighting between the outputs and the inputs in the cost function. The two outputs have an equal weight as do the two inputs. If a large value of q is chosen then the states will be tightly regulated at the cost of large control action which may saturate the actuators.

Figure 5.2 shows the frequency response of a horizontal axis LQG controller designed with the above method. The left plots show the response of u_{hl} to y_{hl} while the right plots show the response of u_{hr} to y_{hl}. The response at the right end of the shaft is very similar to the left end and the vertical controller is similar to the horizontal controller. These plots show that the controllers are multivariable in that they take control action at both horizontal plant inputs in response to a plant output change at only the left end. This is in contrast to the single input, single output built-in compensators described in Section 5.2. The frequency response of the built-in compensators is similar to the u_{hl}/y_{hl} LQG response except that the LQG response has a deep notch at the resonant frequency. This notch should effectively damp out the large resonant peak in the plant as found in the modeling in Chapter 4 and shown in Figure 4.5 and Figure 4.7.

Stable horizontal and vertical controllers were designed with q set to 2.5, 1000 and 4×10^5. The test results are presented in Chapter 6.

5.5 Discrete Sliding Mode Controller

The DSMC (see DeCarlo et al, 1996; Pieper & Surgenor, 1993; Rundell et al, 1996; Slotine & Li, 1991; Utkin, 1977) requires an estimate of the current states, $\hat{x}_k$, to produce a control action u_k. The Kalman filter discussed in Section 5.3 uses the current plant output,

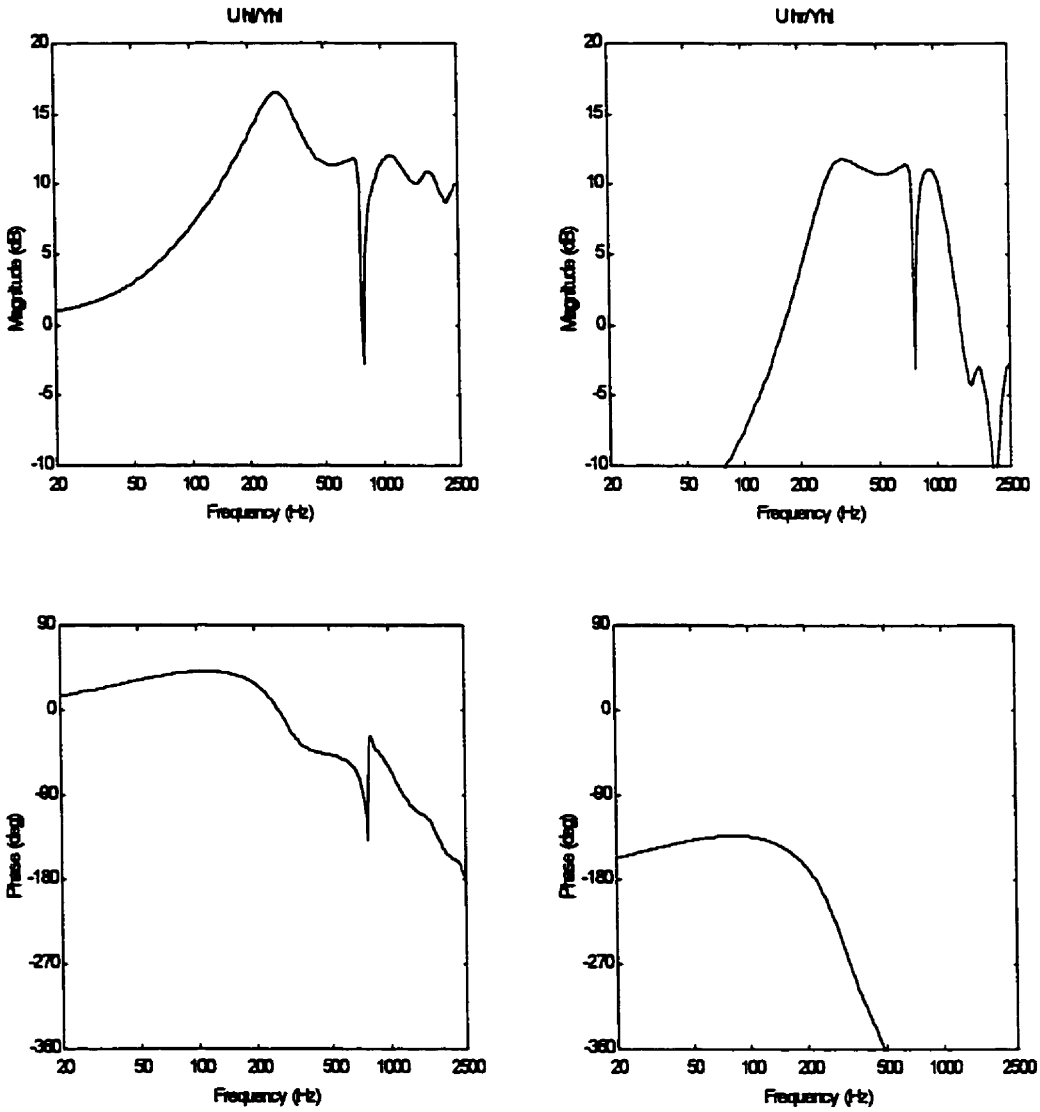

Figure 5.2 Frequency Response of LQG Controller ($q = 1000$) for Horizontal Axis

y_k, and the current plant input, u_k, to produce the estimate $\hat{x}_k$. The LQ controller and the Kalman filter were merged to produce a two input, two output LQG controller but this is not possible with the non-linearities in the DSMC. The Kalman filter and the DSMC cannot be connected in their present form since the state estimate, $\hat{x}_k$, would depend on the control action u_k while u_k would depend on $\hat{x}_k$ producing an algebraic loop in the calculations.

To remove the algebraic loop, a delay must be inserted into the signal flow as shown in Figure 5.3. The control action, u_k, is delayed one sample interval before it is sent to the plant and to the Kalman filter. With this delay inserted the DSMC is controlling a plant with different dynamics which must be reflected in the model. The identified horizontal model was given in equations 4.18 and 4.19.

The input to the model is delayed through the two new states, z_h, that have been added in the following equations

$$z_{h,k+1} = u_{h,k} \tag{5.29}$$

$$x_{h,k+1} = \Phi_h x_{h,k} + \Gamma_h z_{h,k} \tag{5.30}$$

$$y_{h,k} = H_h x_{h,k} \tag{5.31}$$

Equations 5.29 to 5.31 can be merged into a new state space model given by:

$$\begin{bmatrix} x_h \\ z_h \end{bmatrix}_{k+1} = \begin{bmatrix} \Phi_h & \Gamma_h \\ 0_{2\times 16} & 0_{2\times 2} \end{bmatrix} \begin{bmatrix} x_h \\ z_h \end{bmatrix}_k + \begin{bmatrix} 0_{16\times 2} \\ I_2 \end{bmatrix} u_{h,k} \tag{5.32}$$

$$y_{h,k} = \begin{bmatrix} H_h & 0_{2\times 2} \end{bmatrix} \begin{bmatrix} x_h \\ z_h \end{bmatrix}_k \tag{5.33}$$

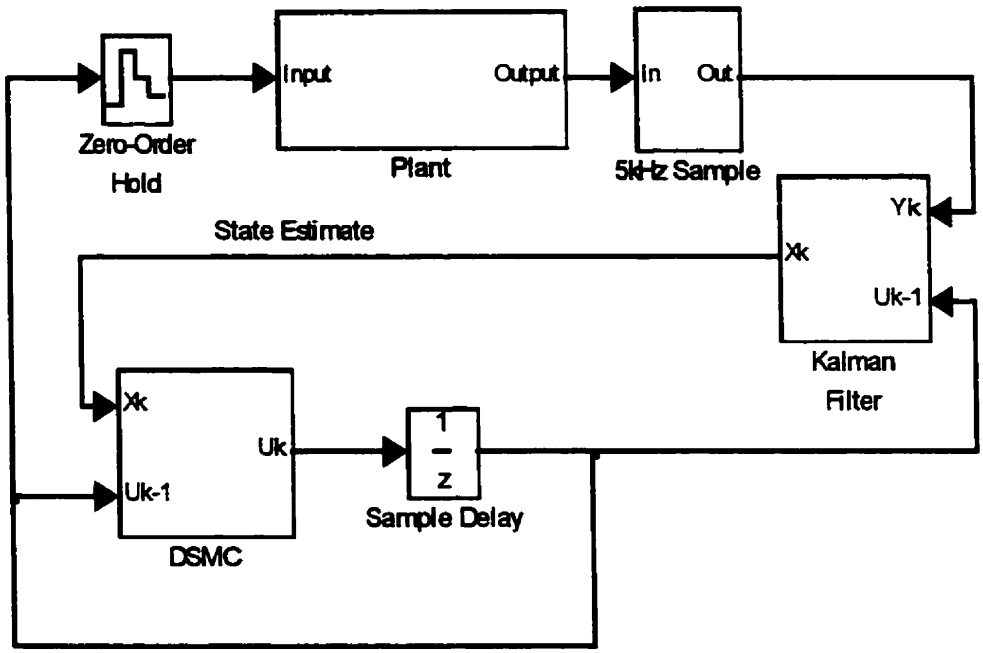

Figure 5.3 DSMC Control Signal Flow

Equations 5.32 and 5.33 delay the input to the original states, x_h, by one sample which is equivalent to using a delayed input, $u_{h,k-1}$, to the model. The controller and estimator based on this new model can be connected as shown in Figure 5.3. The Kalman filter is as designed in Section 5.3. The DSMC can be designed using this delayed input model and implemented using the signal flow in Figure 5.3.

5.5.1 Control Law

The DSMC law for a single control is given by Pieper & Surgenor, 1993:

$$u_k = (K_{eq} + K_{sw})\, x_k \tag{5.34}$$

$$K_{eq} = -[C\Gamma]^{-1} C\,[\Phi - I_n] \tag{5.35}$$

$$K_{sw} = (\phi_{1,k} \cdots \phi_{n,k}) \tag{5.36}$$

$$\phi_{i,k} = \begin{Bmatrix} -\phi.sign\,(s_k x_{i,k}) & |s_k| > \frac{1}{2}(\phi + \bar{v})\, C\Gamma \|x_k\|_1 \\ 0 & otherwise \end{Bmatrix} \tag{5.37}$$

Where:

n is the order of the plant

K_{eq} is the equivalent control matrix $(1 \times n)$

K_{sw} is the switching control matrix $(1 \times n)$

C is the sliding surface matrix $(1 \times n)$

Γ is the system input matrix $(n \times 1)$

s_k is the distance to the sliding surface, $s_k = Cx_k$ $(scalar)$

$\bar{v}$ is the maximum perturbation $(scalar)$

$\|x_k\|_1 = \sum_{i=1}^{n} |x_{i,k}|$, the first norm of the states $(scalar)$

ϕ is the switching strength subject to $\bar{v} < \phi < \left|\frac{2}{C\Gamma}\right| - \bar{v}$ $(scalar)$

The switching control forces the states of the plant onto the sliding surface defined by C while the equivalent control moves the states along the surface towards the origin. The above control law ensures that the switching control is not too strong to overshoot the sliding sector but also sufficient to cause the system to move towards the sliding sector

in the face of disturbances. The DSMC takes into account the sampling rate whereas the robustness of the continuous time sliding mode controller is not guaranteed with a discrete implementation. This is especially important in this application since the sampling rate is slow relative to the first critical frequency of the shaft. The following section details a sliding surface design method to ensure that the sliding surface is stable and the states slide towards the origin.

5.5.2 Sliding Surface Design

The sliding surface was designed to minimize a cost function with relative weighting of the states of the model in equations 5.32 and 5.33. The cost function is written as:

$$J = \sum_{k=0}^{\infty} \begin{bmatrix} x_h \\ z_h \end{bmatrix}_k^T \begin{bmatrix} Q_{11} & Q_{12} \\ Q_{21} & Q_{22} \end{bmatrix} \begin{bmatrix} x_h \\ z_h \end{bmatrix}_k \tag{5.38}$$

$$J = \sum_{k=0}^{\infty} x_{h,k}^T Q_{11} x_{h,k} + x_{h,k}^T Q_{12} z_{h,k} + z_{h,k}^T Q_{21} x_{h,k} + z_{h,k}^T Q_{22} z_{h,k} \tag{5.39}$$

The off-diagonal terms $Q_{12} = Q_{21}^T = 0$ since they have no physical significance. The other terms were chosen so that:

$$J = \sum_{k=0}^{\infty} q x_{h,k}^T H_h^T H_h x_{h,k} + r z_{h,k}^T z_{h,k} \tag{5.40}$$

which is equivalent to:

$$J = \sum_{k=0}^{\infty} q y_{h,k}^T y_{h,k} + r u_{h,k}^T u_{h,k} \tag{5.41}$$

The sliding surface design is reduced to choosing the relative weight of the output, q, and the weight on the control, r.

The sliding surface matrix is given by:

$$C = \left[-\left(K + Q_{22}^{-1}Q_{21}\right) \quad I_2 \right] \tag{5.42}$$

Φ is partitioned as in equation 5.43 so that the Φ_{22} matrix is 2×2 and the other elements of the partition conform in size.

$$\Phi = \begin{bmatrix} \Phi_{11} & \Phi_{21} \\ \Phi_{21} & \Phi_{22} \end{bmatrix} \tag{5.43}$$

The matrix K is given by:

$$K = \left(Q_{22} + \Phi_{12}^T S \Phi_{12}\right)^{-1} \Phi_{12}^T S \Phi^* \tag{5.44}$$

and

$$0 = S - \Phi^{*T} S \Phi^* + \Phi^{*T} S \Phi_{12} R^{-1} \Phi_{12}^T S \Phi^* - Q^* \tag{5.45}$$

$$R = Q_{22} + \Phi_{12}^T S \Phi_{12} \tag{5.46}$$

where

$$\Phi^* = \Phi_{11} - \Phi_{12} Q_{22}^{-1} Q_{21} \tag{5.47}$$

$$Q^* = Q_{11} - Q_{12} Q_{22}^{-1} Q_{21} \tag{5.48}$$

5.5.3 Controller Synthesis

The control law in Section 5.5.1 was implemented for each of the plant inputs for both axes. The sliding surface design parameters q and r were chosen and the sliding surface matrix C was calculated for each axis using the models from Section 4.4 modified to equations 5.32 and 5.33 to account for the introduced delay. The DSMC law in equations 5.34 to 5.37 is for a single control so for each axis the sliding surface matrix, C, was partitioned into two row vectors (one for each control input). The model input matrix, Γ_h, was partitioned into two column vectors so that the control law in equations 5.34 to 5.37 could be implemented for both of the plant inputs for both of the models.

The tuning of the controllers was done by choosing $\bar{v}$ to be 0.005 and ϕ to be 0.01 followed by choosing the cost function parameters q and r. It was found that a closed loop stable system was more easily tuned with a lower switching strength, ϕ. The relative magnitude of q and r determines the level of regulation versus the amount of control action taken. The control action weight, r, was set to 50. If q was chosen to be too large then the control action would often saturate leading to instabilities. Lower values of q would result in the closed loop plant resonating at the first resonant frequency. A value of q between 50 and 500 was found to produce good results.

5.5.4 Proportional-Integral Control

A PI controller was added to the DSMC to improve the reference tracking performance of the closed loop system. The reference inputs and the PI controllers were con-

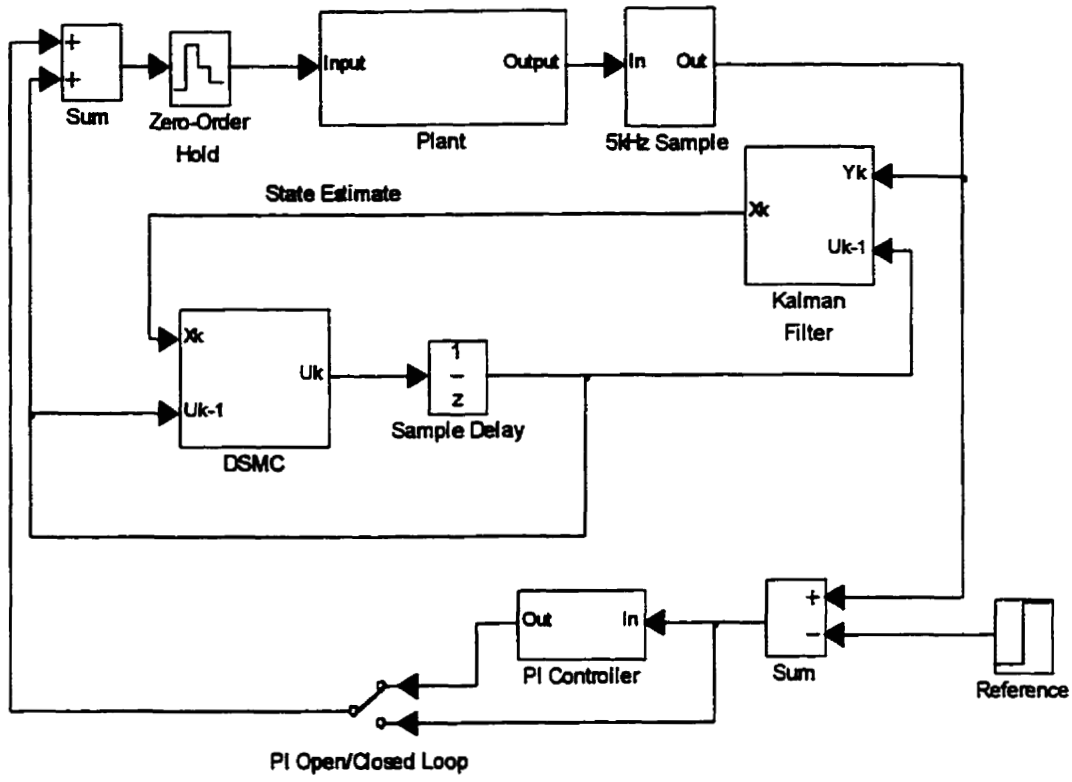

Figure 5.4 Control Flow of DSMC and PI Controller for One Axis

nected in the configuration shown in Figure 5.4 for each of the horizontal and vertical controllers.

The dynamics of the plant were measured by stepping one of the reference inputs with the PI controller in open loop and the DSMC levitating the shaft. The left horizontal step test is shown in Figure 5.5. From the step tests, the time constant and steady state gain of the response can be measured to approximate the DSMC closed loop system as first order with the model:

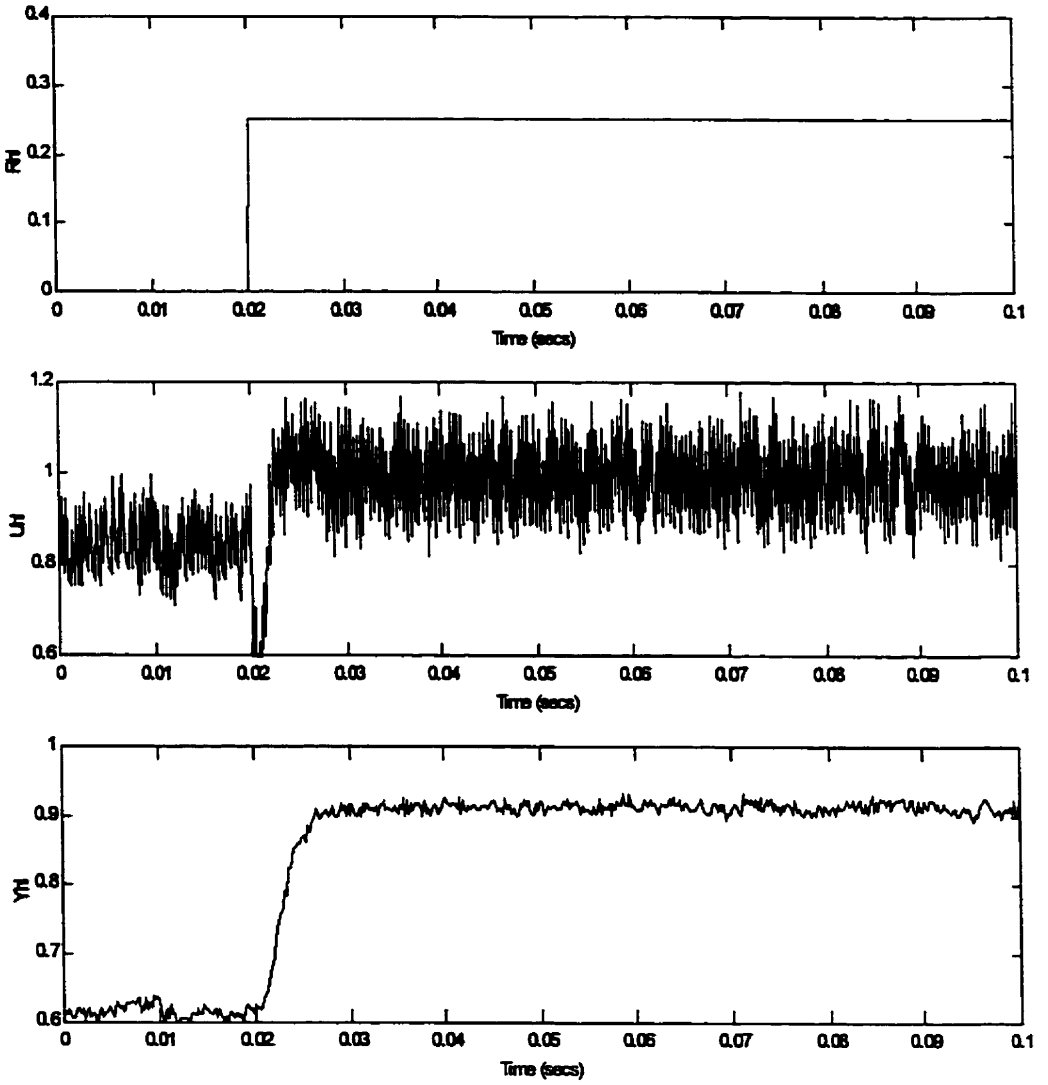

Figure 5.5 Reference Step Response of Left Horizontal DSMC (Top: Reference, Middle: Input, Bottom: Output)

$$G(s) = \frac{K_p}{\tau s + 1} \tag{5.49}$$

where:

K_p is the process gain ($K_p = 2$ for the left horizontal)

and τ is the time constant ($\tau \simeq 0.005 secs$ for the left horizontal)

The PI controller was then tuned using the Lambda tuning method (Åström & Hägglund, 1995) to produce a designed closed loop time constant, λ. The PI controller has the transfer function:

$$C(s) = \frac{K_c (T_r s + 1)}{T_r s} \tag{5.50}$$

where:

K_c is the proportional control gain

and Tr is the reset time of the integrating action

With the following tuning:

$$K_c = \frac{\tau}{K_p \lambda} \tag{5.51}$$

$$T_r = \tau \tag{5.52}$$

the closed loop transfer function is:

$$G_{cl}(s) = \frac{GC}{1 + GC} = \frac{1}{\lambda s + 1} \tag{5.53}$$

This allows the PI controller to be tuned significantly slower than the DSMC so that there is negligible interaction and fighting between the two controllers. All of the

PI controllers were tuned with the same closed loop time constant of $\lambda = 0.015secs$. Reference steps were made with the tuned PI controllers and the left horizontal response is shown in Figure 5.6. With the PI controllers in closed loop, the steady state output tracks the reference with no offset. The response also reaches the steady state value at about 0.06secs after the reference change was made indicating that the tuning produced the desired closed loop time constant, that is a settling time of four time constants.

5.5.5 Switched Sliding Surface Controller

To reduce the chance of the shaft touching the housing, a DSMC was designed to take more aggressive control action when a position measurement deviated a large distance from the zero position. A cut-off band of 0.5 Volts was used to determine which controller tuning should be used. The operation of the horizontal controller had three tunings of the cost function but used the same choices of the other parameter as in Section 5.5.3. The cost function in equation 5.40 was modified to the form:

$$J = \sum_{k=0}^{\infty} q_1 x_{h,k}^T H_1^T H_1 x_{h,k} + q_2 x_{h,k}^T H_2^T H_2 x_{h,k} + r z_{h,k}^T z_{h,k} \tag{5.54}$$

$$J = \sum_{k=0}^{\infty} q_1 y_{hl,k}^2 + q_2 y_{hr,k}^2 + r u_{h,k}^T u_{h,k} \tag{5.55}$$

where:

$H_h = \begin{bmatrix} H_1 \\ H_2 \end{bmatrix}$ are the two rows of the model output equation.

and q_1, q_2, and r are the tuning parameters

Three different sets of parameters were used in the cost function shown in Table 5.1. The tuning choices in Table 5.1 were made so that if one end of one axis move out of the

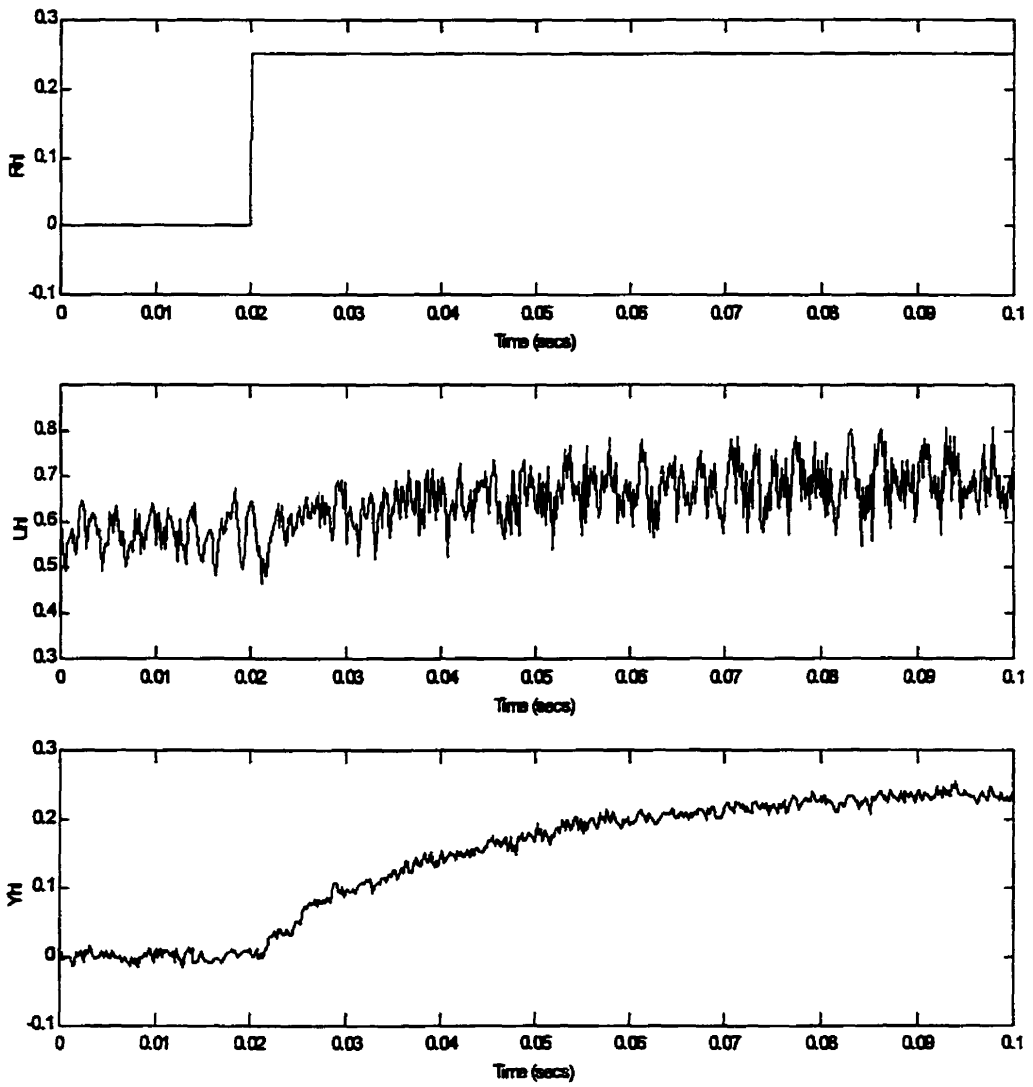

Figure 5.6 Left Horizontal Reference Step Response of DSMC with PI (Top: Reference, Middle: Input, Bottom: Output)

y_{hl}	y_{hr}	q_1	q_2	r
$< \pm 0.5$	$< \pm 0.5$	100	100	50
$> \pm 0.5$	$< \pm 0.5$	100	1	50
$< \pm 0.5$	$> \pm 0.5$	1	100	50
$< \pm 0.5$	$< \pm 0.5$	100	100	50

Table 5.1 DSMC Switched Surface Tunings and Conditions for Each Tuning Use

0.5 band then a tuning with a larger relative weight on output deviation associated with that end is used. This will attempt to use more control action to move that end back into the band possibly at the expense of the position of the other end. When both outputs are within the band then the equally weighted tuning is used. When both ends of the shaft are out of the band, which would happen at lift-off, the equally weighted tuning is also used. This was done because it was found that the control signal saturated on lift off with the normal tuning and more aggressive tuning would not help this condition.

The values of q_1 and q_2 when one end is out of the band were chosen to be between saturating the control and the original central level. With too large a difference between q_1 and q_2, the controller would get into a cycle where a large control action was used to move one end back into the band while the opposite end fell out of the band repeating the cycle. This controller was difficult to tune since there are many parameter choices that must be made.

5.6 Summary

This chapter presented the nominal design of the built-in compensators. Two discrete control algorithms were designed using the parameter estimated model with a modified

resonant pole developed in the previous chapter. A Kalman filter was designed to estimate the states of the plant since both of the discrete controllers rely on state feedback.

An LQ controller was designed using a cost function which reflected the goal of regulating the shaft position without saturating the control input. The controller was combined with a Kalman filter to form an LQG controller and was found to be stable with several different tuning choices.

In the design of the DSMC the interconnection between the DSMC and the Kalman filter caused an algebraic loop that was removed by an inserted delay but meant that the model of the plant had to be modified to include a unit delay in the control action input. The DSMC was designed using this modified model and a cost function which reflected the same goals as the LQG controller. The DSMC was difficult to tune since there were several parameter choices to be made. A range of cost functions were found to produce a stable controller.

PI controllers were added to the DSMC to improve the reference tracking performance of the closed loop system. The PI controllers were tuned to be significantly slower than the DSMC controller to avoid the controllers interacting. The DSMC was also modified to use a more aggressive control action when one end of the shaft moved away from the zero position. This controller was difficult to tune since it has more parameters.

Chapter 6
Experimental Results

6.1 Introduction

In this chapter the operating performance of the closed loop systems with the control laws developed in Chapter 5 are evaluated experimentally. First there is a brief discussion on the evaluation criteria for the controllers as well as a discussion on the need to scale the recorded voltage data. The following controllers were tested:

- The built-in compensators discussed in Section 5.2.
- The LQG controller developed in Section 5.4.
- The DSMC-PI controller developed in Section 5.5.
- The DSMC-PI controller with a switching sliding surface developed in Section 5.5.5.

Three different sets of tuning parameters were tested with the LQG and the DSMC-PI controllers. The DSMC-PI controller with variable surfaces was also tested with one set of tuning parameters. The test results were compared to evaluate the performance of the different controlled systems. The design and implementation of the controllers can also be verified by observing the effect of different tuning choices on the controller performance.

Each controller was tested under the following conditions:

A. The left horizontal end of the shaft was tapped with a metal pendulum and the integration of the squared plant outputs and inputs were recorded.

B. A mass was added to the shaft and test A was repeated.

C. White noise was added to the control signal and the variance of the plant outputs and control action were calculated.

D. The shaft was imbalanced with a mass then spun at about 10,000 rpm while the variance of the plant outputs and control action were recorded.

6.2 Closed Loop System Evaluation Criteria

With the experimental test apparatus used in this research there is no final industrial implementation and hence no precise control objectives. The main requirement of this controller is that it levitates the shaft under varying operating conditions. The shaft motion should not meet the hard limits imposed by the bearing sizes. That is, the shaft should stay within the frame without hitting the walls of the bearing. The final application would determine what operating conditions are important and how to quantify how well the shaft is levitated. For example, is the operation of the bearing with a varying shaft mass important? Is preventing shaft touchdown more important than reducing just the shaft position variance? Is the actuator power consumption important compared to position regulation? Is reference tracking important?

There are other considerations in evaluating a control strategy not directly related to controller performance. These would include controller complexity, tuning difficulty, and

hardware requirements. The experimental results presented in this chapter are aimed at demonstrating how the designed controllers can be tuned for different closed loop performance. The tuning values were chosen to demonstrate the large variation in performance that can be achieved by the controllers. Actual implementations can then use this data to guide tuning for given environments.

6.3 Signal Scaling

The voltage signals of the apparatus are in the range of $0V$ to $\pm 5V$ for the inputs and $\pm 5V$ for the outputs. The signals were scaled to have more physical significance in the data analysis. Each input to the apparatus controls the corresponding electromagnet current to a scale of $0.25A/V$. The inputs to the apparatus were multiplied by 0.25 to reflect this scaling. The scaling of the output signals were chosen to reflect a possible control objective. Each output was multiplied by $\sqrt{0.4}/0.1$ so that an output of 0.5 would correspond to a squared value of 10 (i.e. $\left(0.5 \times \sqrt{0.4}/0.1\right)^2 = 10$) reflecting a higher concern for this large deviation. An output of approximately 0.158 scaled and squared would result in a value of 1. Any value below 0.158 scaled and squared would be reduced reflecting a lower concern for small deviations.

6.4 Shaft Taps

The shaft was tapped with a metal pendulum near the left end of the shaft in approximately a horizontal direction. The results show that there was some vertical component to

the tap. The pendulum was drawn back to a fixed position on each tap by means of a jig to keep the taps consistent for all controllers. Each controller was tapped 75 times and the plant inputs and outputs were recorded and scaled.

The integration of the deviation of the inputs and outputs due to the tap was calculated by taking a window of data surrounding the tap time. For each recorded signal, the data leading up to the tap was averaged to find the steady state shaft position and this value was subtracted from all data in the window. The squared integration of the window of data was then calculated by summing the squared values of the scaled data over the whole window multiplied by the sample period. The mean of the integration of the 75 taps along with their standard deviations are presented in Sections 6.4.1 to 6.4.4.

The time plots of the tap response shown in Figure 6.1 to Figure 6.11 are for illustrative purposes and are not the actual data windows used to integrate the response. The data is shown in its recorded form of volts with the vertical axis span constant for all input plots and constant for all output plots. The time span for all plots are the same. In all cases, the four control actions (horizontal left, horizontal right, vertical left and vertical right) are shown down the left side of the sets of plots while the outputs (horizontal left, horizontal right, vertical left and vertical right) are shown down the right side.

6.4.1 Built-In Compensators

The plots in Figure 6.1 show a large response at the right end of the shaft to the tap at the left end which can also be seen in the integration of y_{hl} and y_{hr} in Table 6.1. The SISO nature of the compensators means that the control action taken at the left horizontal

actuator in response to the tap affected the right horizontal output via the shaft dynamics. The right horizontal actuator response in turn affected the left horizontal output with the net result of oscillations in the two horizontal outputs.

6.4.2 LQG Controller

Three LQG controllers were designed with the tuning parameter q (from Section 5.4) set to 2.5, 1000 and 4×10^5 corresponding to an increasing cost on output deviation. The measured output integration in Table 6.2 decreases with increasing q. The responses in Figure 6.2 to Figure 6.4 also show that a controller with an increasing value of q has a smaller initial peak in the left horizontal output due to a stronger control action. This is consistent with the desired effect of the tuning.

The controller with q set to 2.5 did not respond very quickly to the taps and slowly returned the shaft back to the steady state position. With q set to 4×10^5, the control action is fast and noisy as the more aggressive tuning tried to react quickly to all of the smaller deviations in the position measurement. There is no performance increase when q is increased from 1000 to 4×10^5 but the control action is more aggressive as seen in Figure 6.3 and Figure 6.4 and more control energy is used as shown in Table 6.2.

The steady position of the shaft is not usually at zero since there is no integrating action in the controller. A constant bias must be added to the inputs to move the outputs to a near-zero steady position.

	Mean ($\times 10^{-3}$)	Standard Deviation ($\times 10^{-3}$)		Mean	Standard Deviation
u_{hl}	0.51	0.02	y_{hl}	0.28	0.01
u_{hr}	0.28	0.01	y_{hr}	0.14	0.006
u_{vl}	0.017	0.001	y_{vl}	0.0086	0.0005
u_{vr}	0.012	0.002	y_{vr}	0.0068	0.001

Table 6.1 Integration of Scaled Squared Signal of Built-In Compensator Response to Horizontal Taps at Left End of Shaft

q = 2.5

	Mean($\times 10^{-3}$)	Standard Deviation($\times 10^{-3}$)		Mean	Standard Deviation
u_{hl}	1.11	0.05	y_{hl}	1.12	0.05
u_{hr}	0.10	0.004	y_{hr}	0.70	0.003
u_{vl}	0.070	0.003	y_{vl}	0.083	0.004
u_{vr}	0.0028	0.0005	y_{vr}	0.0040	0.0007

q = 1000

	Mean($\times 10^{-3}$)	Standard Deviation($\times 10^{-3}$)		Mean	Standard Deviation
u_{hl}	0.74	0.06	y_{hl}	0.19	0.02
u_{hr}	0.091	0.007	y_{hr}	0.010	0.0008
u_{vl}	0.16	0.001	y_{vl}	0.0057	0.0004
u_{vr}	0.0071	0.001	y_{vr}	0.00069	0.0001

q = 4×10^5

	Mean($\times 10^{-3}$)	Standard Deviation($\times 10^{-3}$)		Mean	Standard Deviation
u_{hl}	0.95	0.1	y_{hl}	0.19	0.03
u_{hr}	0.23	0.03	y_{hr}	0.011	0.002
u_{vl}	0.038	0.007	y_{vl}	0.0052	0.0007
u_{vr}	0.030	0.009	y_{vr}	0.0010	0.0004

Table 6.2 Integration of Scaled Squared Signal of LQG Controllers Response to a Horizontal Tap at Left End of Shaft

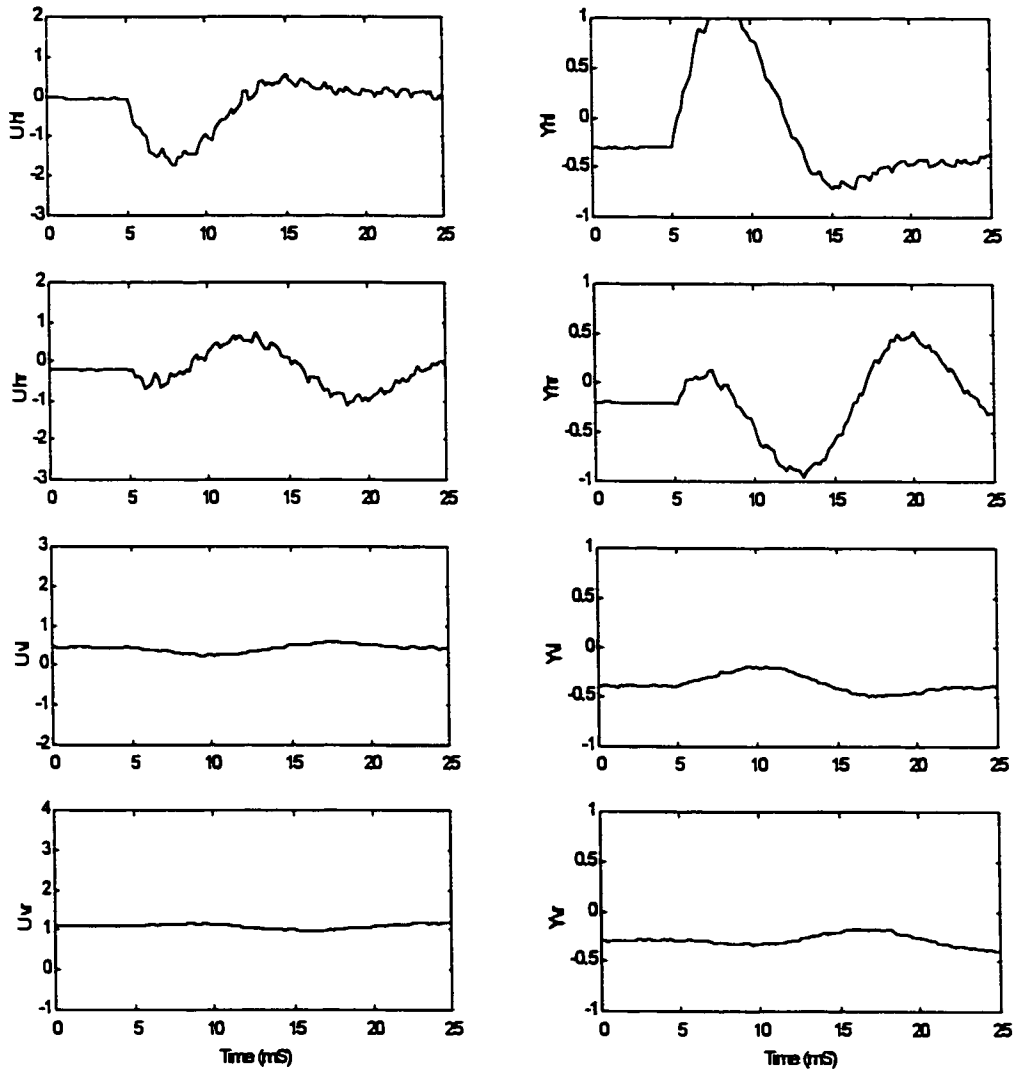

Figure 6.1 Built-In Compensator Response to a Horizontal Tap at Left End of Shaft (Verical Axes in Volts, Horizontal Axes in Milliseconds)

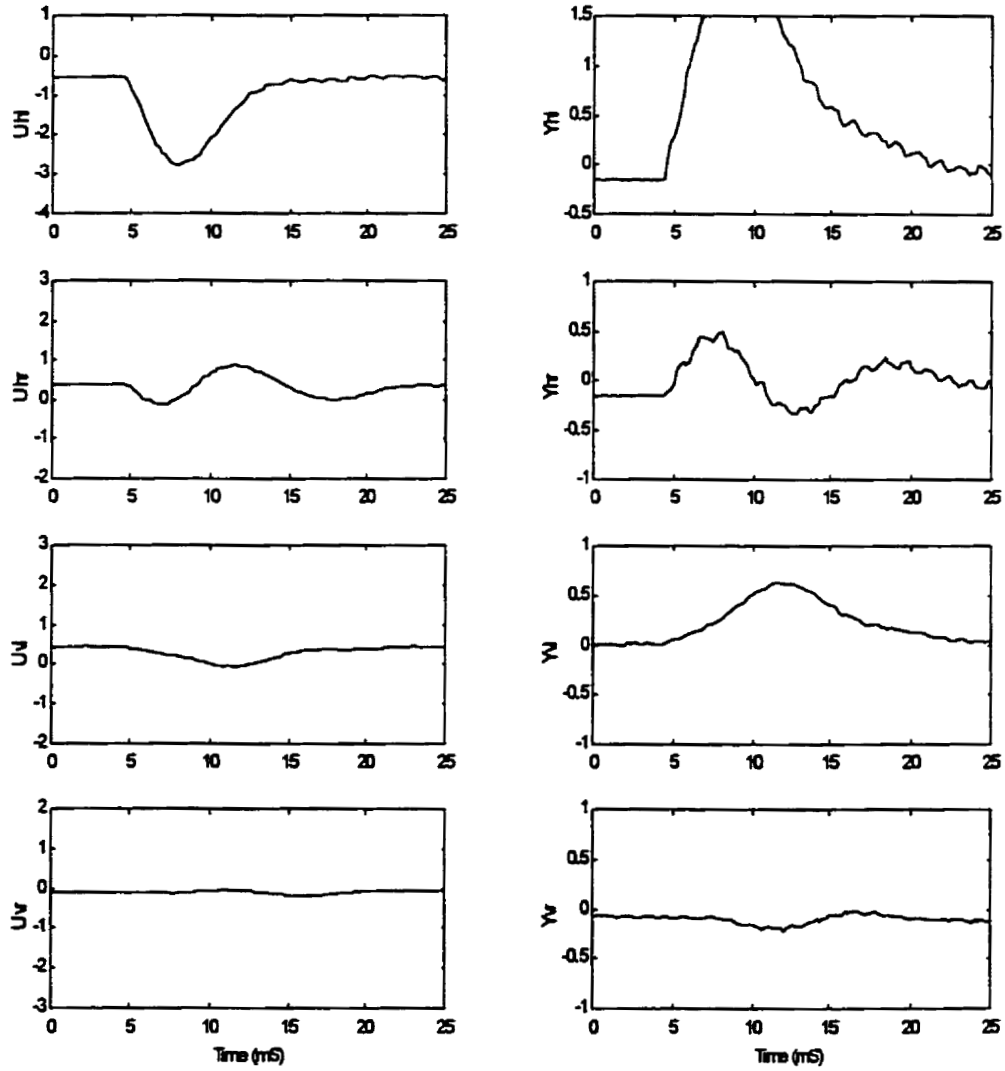

Figure 6.2 LQG Controller ($q = 2.5$) Response to a Horizontal Tap at Left End of Shaft (Verical Axes in Volts, Horizontal Axes in Milliseconds)

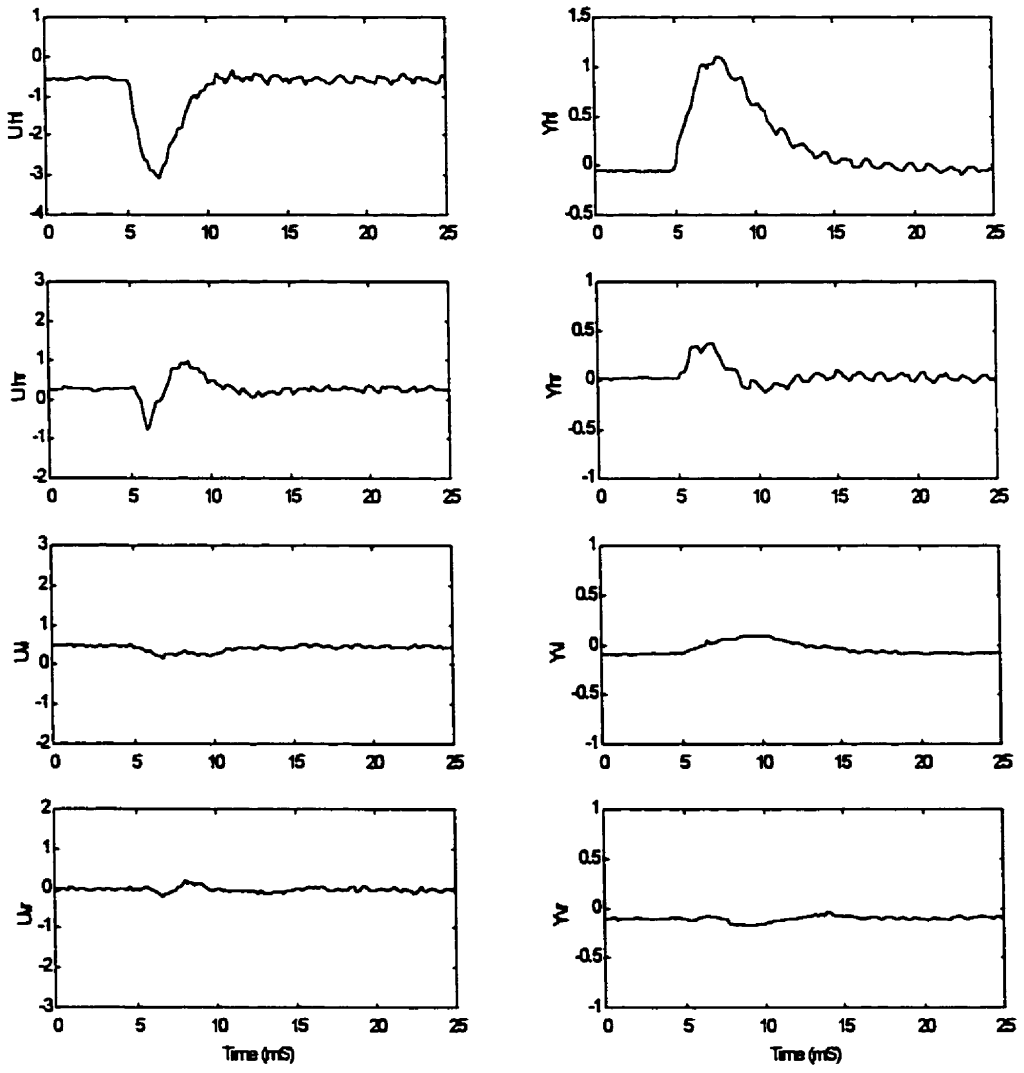

Figure 6.3 LQG Controller ($q = 1000$) Response to a Horizontal Tap at Left End of Shaft (Verical Axes in Volts, Horizontal Axes in Milliseconds)

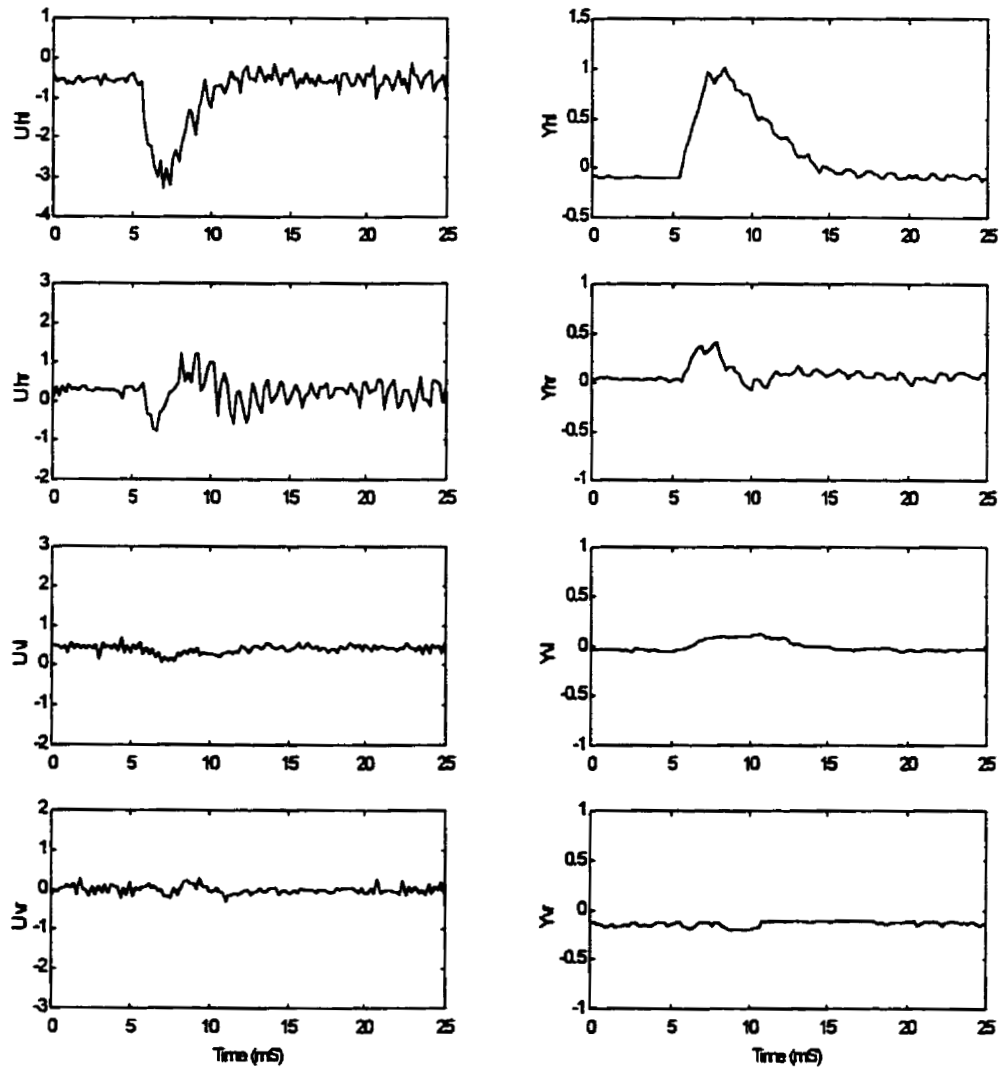

Figure 6.4 LQG Controller ($q = 4 \times 10$) Response to a Horizontal Tap at Left End of Shaft (Verical Axes in Volts, Horizontal Axes in Milliseconds)

6.4.3 DSMC-PI Controller

The results of three DSMC-PI controllers with the tuning parameters q set to 50, 100 and 500 and r set to 50 (as in Section 5.5.1) are shown in Table 6.3 and Figure 6.5, Figure 6.7 and Figure 6.8. These values of q correspond to an increasing weight on output deviation. The tabulated results show that the output deviation decreases and the control action increases with an increasing q while the plots of the responses show an increasing amount of control used and a shorter settling time.

Shown in Figure 6.6 and Figure 6.9 are the two horizontal outputs and the control action of the components of the DSMC-PI controller. These are included to show the difference in control action in the two extremes of tuning as well as the contribution of the different control components. In both cases the PI compensator (the second row of figures) makes only a small contribution due to the relatively slow tuning chosen. Stabilization of the shaft is done by the DSMC and predominantly by the equivalent control component (the fourth row). The switching control action (the third row) could be strengthened by increasing the tuning constant ϕ (see Section 5.5.1) but it was found that it was more difficult to produce a stable or non-oscillating controller with larger values of ϕ.

With q set to 500 the control action becomes more aggressive and although the plant is stable, the response does not settle down as quickly as with the lower values of q. The results with q set to 500 show the lowest deviation of all of the DSMC-PI and LQG controllers for y_{hl}. With $q = 100$, the results are very comparable to the LQG controller with $q = 1000$ and $q = 4 \times 10^5$ although the DSMC-PI controller used more control energy.

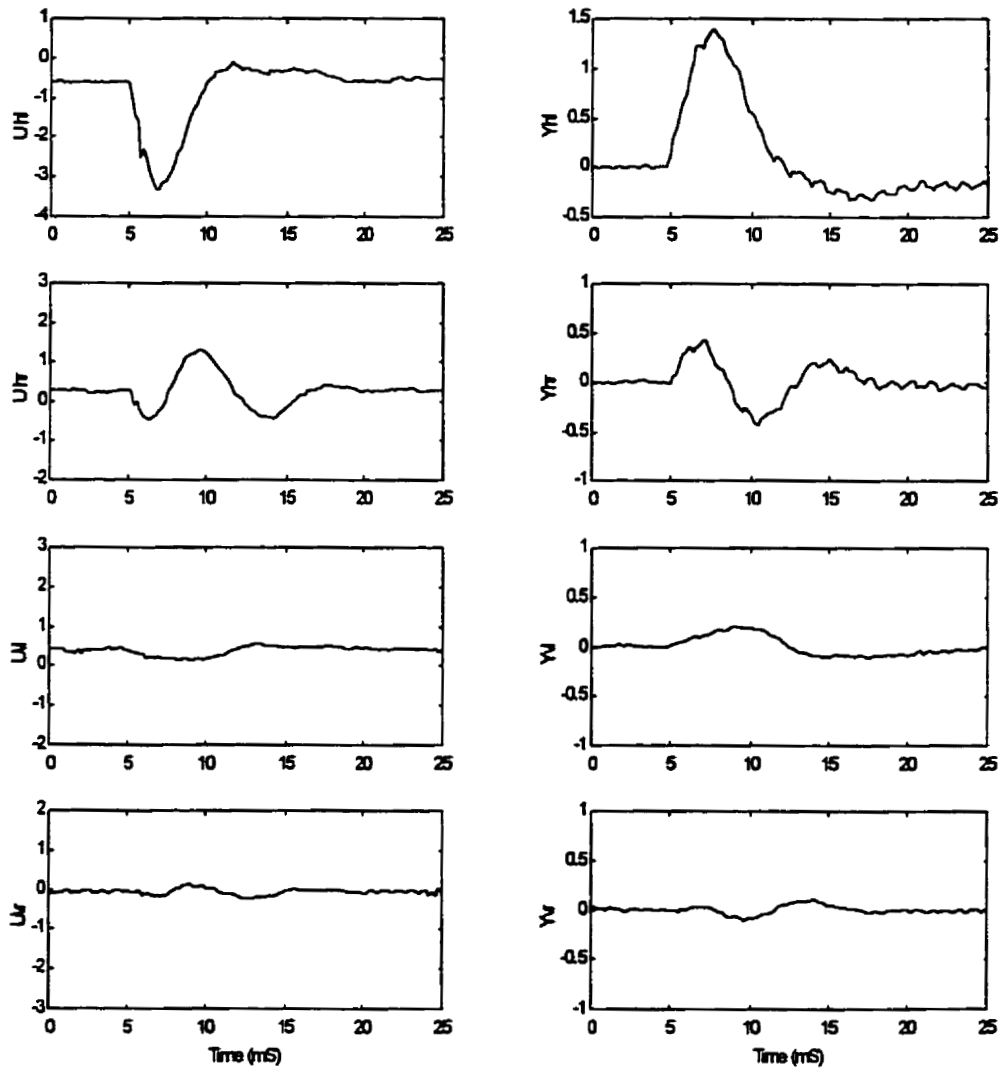

Figure 6.5 DSMC-PI ($q = 50$) Response to a Horizontal Tap at Left End of Shaft (Verical Axes in Volts, Horizontal Axes in Milliseconds)

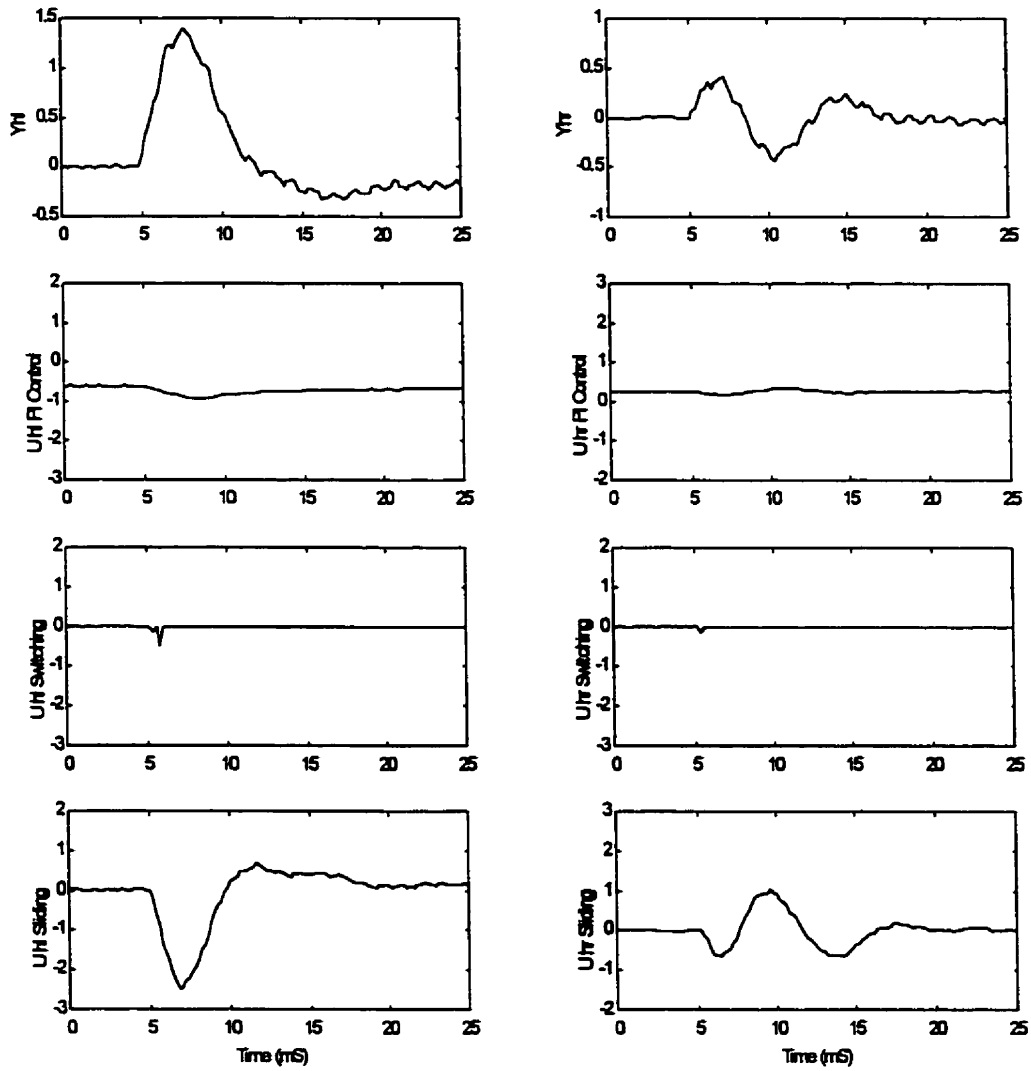

Figure 6.6 DSMC-PI ($q = 50$) Control Action Response to a Horizontal Tap at Left End of Shaft (Verical Axes in Volts, Horizontal Axes in Milliseconds)

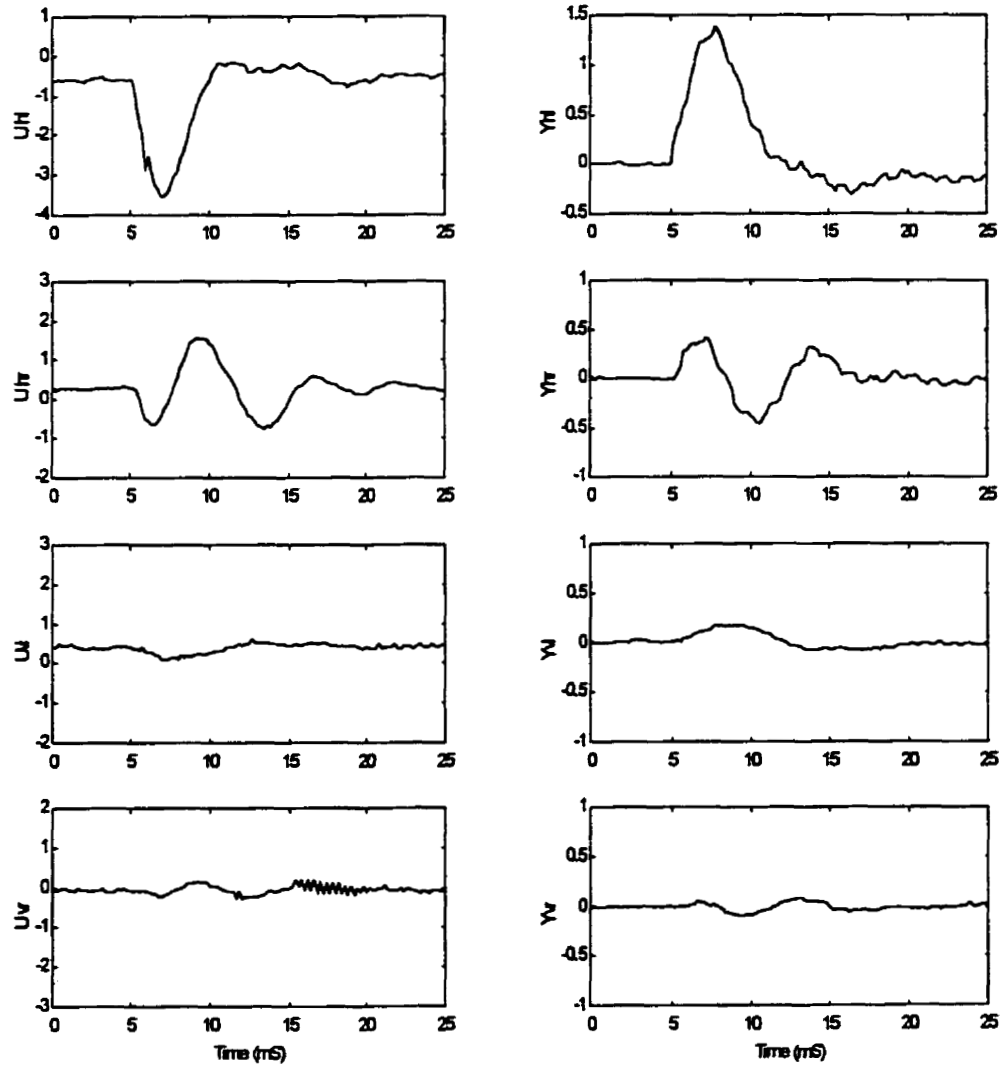

Figure 6.7 DSMC-PI ($q = 100$) Response to a Horizontal Tap at Left End of Shaft (Verical Axes in Volts, Horizontal Axes in Milliseconds)

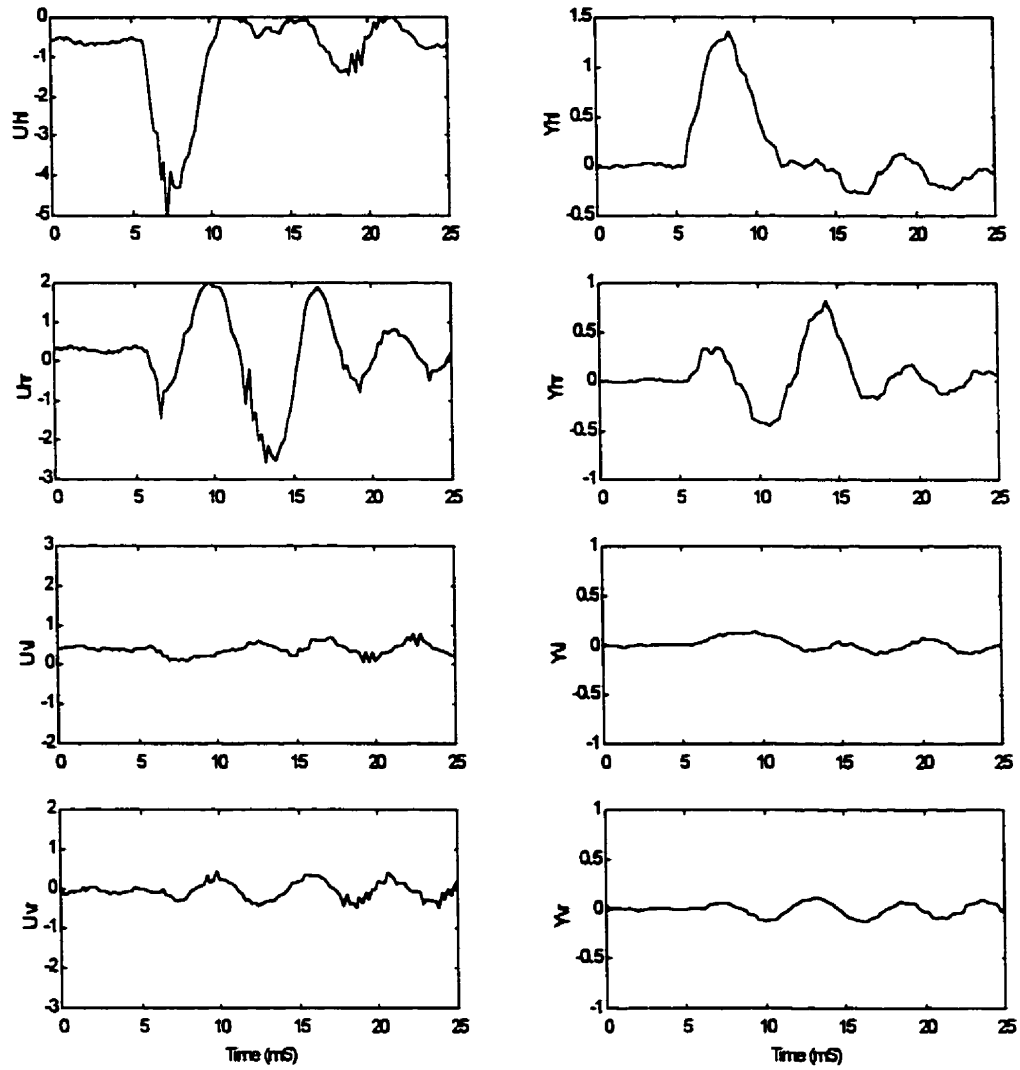

Figure 6.8 DSMC-PI ($q = 500$) Response to a Horizontal Tap at Left End of Shaft (Verical Axes in Volts, Horizontal Axes in Milliseconds)

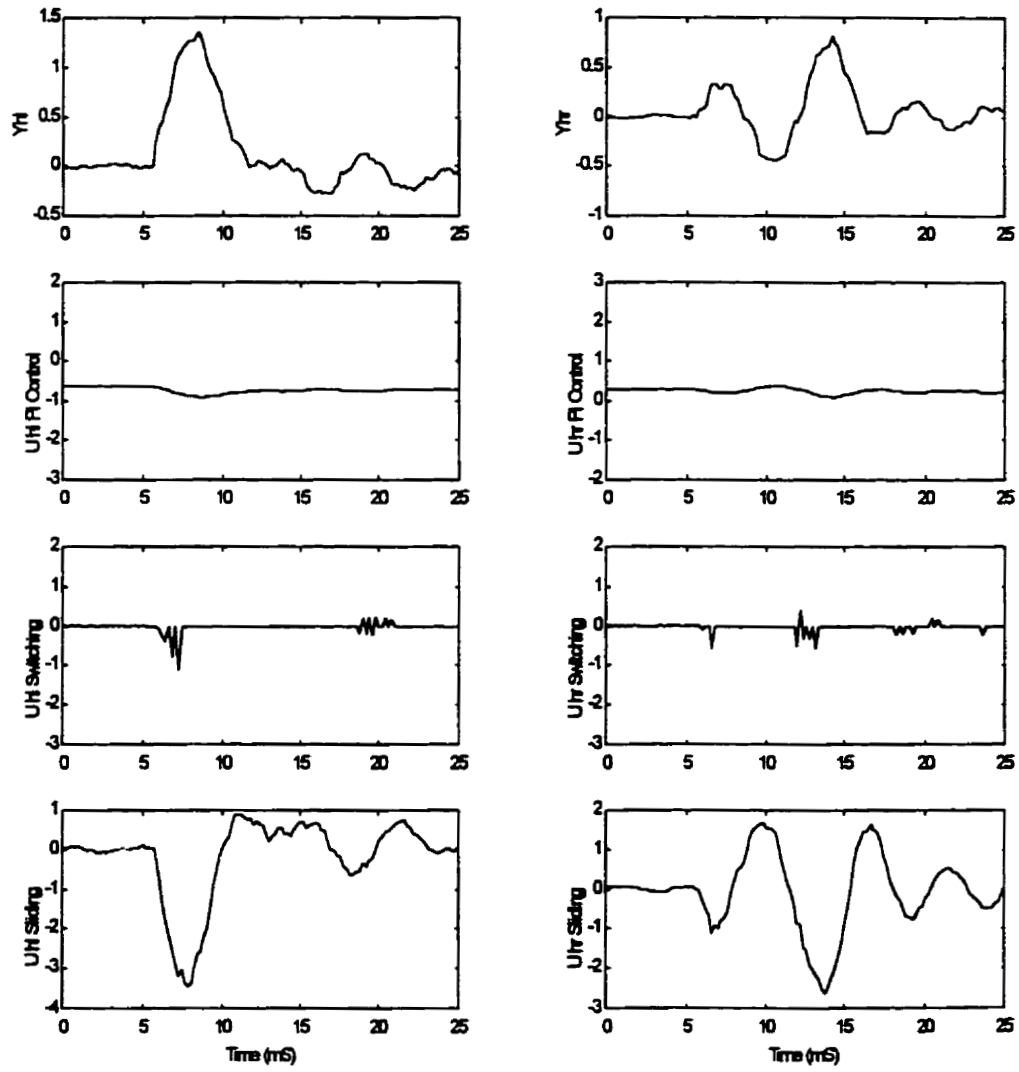

Figure 6.9 DSMC-PI ($q = 500$) Control Action Response to a Horizontal Tap at Left End of Shaft (Verical Axes in Volts, Horizontal Axes in Milliseconds)

6.4.4 DSMC Controller with Switched Surface

The DSMC controller discussed in Section 5.5.5 was tested and the results are shown in Table 6.4, Figure 6.10 and Figure 6.11. In response to a tap, the switched surface design caused the controller to use a stronger control action to move y_{hl} back towards the zero position at the expense of allowing y_{hr} to deviate more than in the case of the DSMC-PI controller with a tuning of $q = 100$ and $r = 50$ (see Figure 6.7 and Figure 6.10). The result is a larger deviation in y_{hr} and some oscillations in the response with a small improvement in the maximum deviation in y_{hl} compared to the DSMC-PI controller with a tuning of $q = 100$ and $r = 50$.

This controller was difficult to tune since there are several more tuning parameters than the DSMC-PI controller with one sliding surface and care was needed to reduce the chance of saturating the actuators.

6.5 Shaft with Added Mass Taps

The mass of the shaft was approximately doubled by taping 235g of lead to it. The mass was located to the left side of center. The shaft was then tapped with the same pendulum setup as in Section 6.4. The same data analysis was performed to measure the deviation of the shaft and the results are presented in Table 6.5 to Table 6.8.

The results cannot be directly compared to Section 6.4 since the added mass acts as a damper to the tap. All of the controllers that were tested were stable with the added mass and the relative performance of the controllers is similar to the results in Section 6.4 with

q = 50

	Mean($\times 10^{-3}$)	Standard Deviation($\times 10^{-3}$)		Mean	Standard Deviation
u_{hl}	0.93	0.06	y_{hl}	0.23	0.02
u_{hr}	0.22	0.01	y_{hr}	0.027	0.002
u_{vl}	0.024	0.002	y_{vl}	0.0087	0.0006
u_{vr}	0.011	0.002	y_{vr}	0.0019	0.0002

q = 100

	Mean($\times 10^{-3}$)	Standard Deviation($\times 10^{-3}$)		Mean	Standard Deviation
u_{hl}	1.09	0.09	y_{hl}	0.20	0.02
u_{hr}	0.35	0.02	y_{hr}	0.029	0.002
u_{vl}	0.023	0.002	y_{vl}	0.0058	0.0005
u_{vr}	0.017	0.002	y_{vr}	0.0018	0.0002

q = 500

	Mean($\times 10^{-3}$)	Standard Deviation($\times 10^{-3}$)		Mean	Standard Deviation
u_{hl}	1.77	0.2	y_{hl}	0.16	0.02
u_{hr}	1.24	0.09	y_{hr}	0.046	0.004
u_{vl}	0.039	0.006	y_{vl}	0.0032	0.0004
u_{vr}	0.073	0.01	y_{vr}	0.0036	0.0006

Table 6.3 Integration of Scaled Squared Signal of DSMC Controller Response to a Horizontal Tap at Left End of Shaft

	Mean($\times 10^{-3}$)	St andard Deviation($\times 10^{-3}$)		Mean	Standard Deviation
u_{hl}	1.19	0.1	y_{hl}	0.23	0.02
u_{hr}	0.66	0.06	y_{hr}	0.080	0.005
u_{vl}	0.022	0.001	y_{vl}	0.0061	0.0004
u_{vr}	0.014	0.002	y_{vr}	0.0017	0.0002

Table 6.4 Integration of Scaled Squared Signal of DSMC Controller with Switched Surface Response to a Horizontal Tap at Left End of Shaft

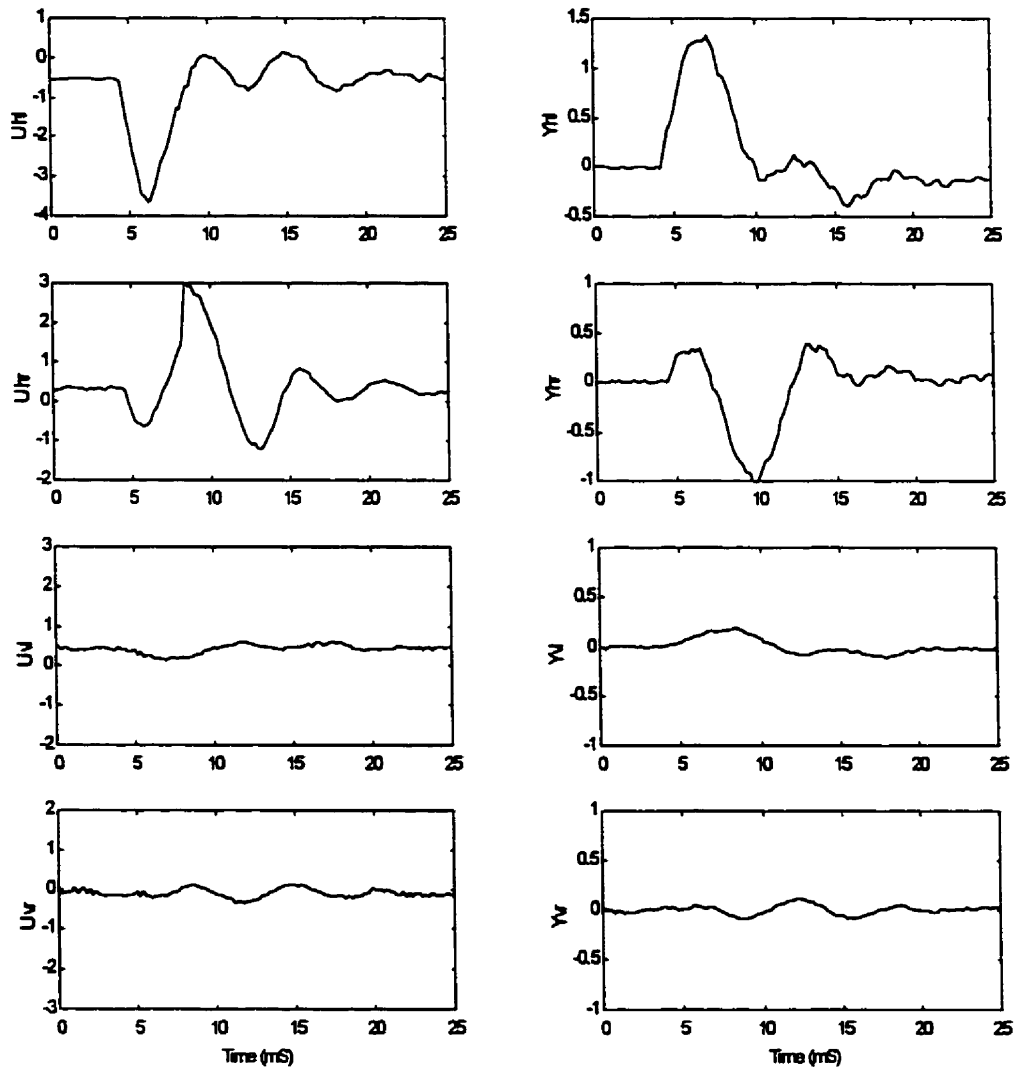

Figure 6.10 DSMC ($q = 100$) with a Switched Sliding Surface Response to a Horizontal Tap at Left End of Shaft (Verical Axes in Volts, Horizontal Axes in Milliseconds)

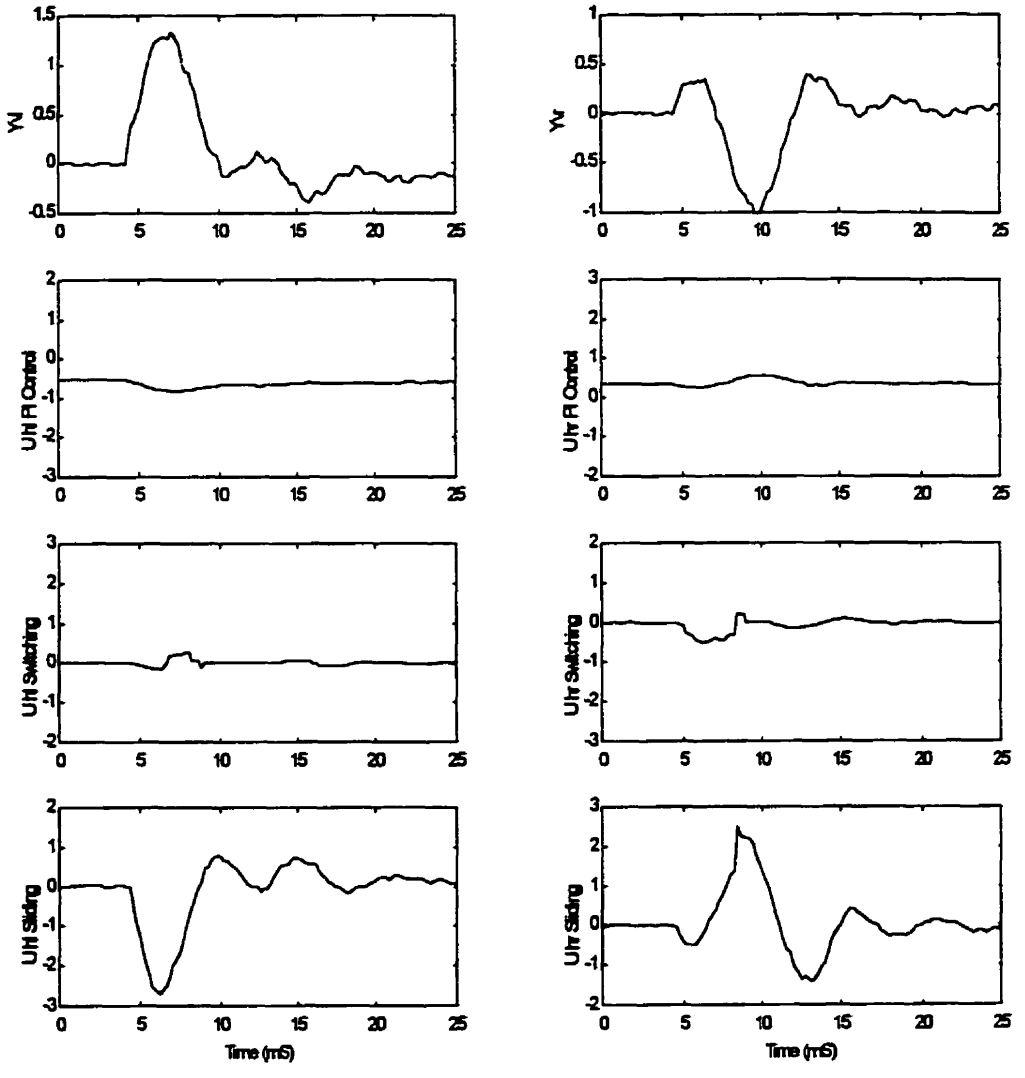

Figure 6.11 DSMC ($q = 100$) with a Switched Sliding Surface Control Action Response to a Horizontal Tap at Left End of Shaft (Verical Axes in Volts, Horizontal Axes in Milliseconds)

two exceptions. The LQG controller with $q = 2.5$ had a tendency for the outputs to drift during normal operation. Without the added mass, y_{hl} for the built-in compensator was 0.28 compared to 0.20 for the DSMC controller with $q = 100$ but with the added mass y_{hl} was 0.38 and 0.24 for the same controllers. The y_{hl} output deviation with the added mass was significantly larger for the built-in compensators relative to the other controllers compared to the tests without the added mass. The performance of the built-in compensators degraded considerably more than the other controllers with the added mass.

6.6 Matched Noise

A matched noise test was performed to evaluate the robustness of the controllers in the presence of large amounts of noise. Uncorrelated Gaussian noise sources (mean:0, variance:0.5) were added to each of the control signals using the Simulink 'Gaussian Noise' block at an output rate of 5kHz. The control inputs and position outputs were recorded for one second and the data was scaled as in Section 6.3. The variances of the input and output data were then calculated and are shown in Table 6.9.

The built-in compensators and the LQG controller with $q = 2.5$ allowed the shaft to touch the bearing housing many times during the test giving an artificially low output variance. From the test results it can be seen the that LQG controllers with larger values of q had the lowest variance of all of the controllers indicating better noise rejection. All of the DSMC-PI controllers kept the shaft from hitting the housing. The DSMC-PI controller with $q = 500$ appeared to use a lot of control action in an attempt to regulate the outputs

	Mean ($\times 10^{-3}$)	Standard Deviation ($\times 10^{-3}$)		Mean	Standard Deviation
u_{hl}	0.65	0.03	y_{hl}	0.38	0.02
u_{hr}	0.41	0.02	y_{hr}	0.22	0.009
u_{vl}	0.031	0.003	y_{vl}	0.014	0.001
u_{vr}	0.069	0.03	y_{vr}	0.029	0.01

Table 6.5 Integration of ScaledSquared Signal of Built In Compensator Response to Horizontal Taps at Left End of Shaft with Added Mass

q = 2.5

	Mean ($\times 10^{-3}$)	Standard Deviation ($\times 10^{-3}$)		Mean	Standard Deviation
u_{hl}	0.92	0.06	y_{hl}	1.12	0.08
u_{hr}	0.15	0.05	y_{hr}	0.13	0.08
u_{vl}	0.52	0.2	y_{vl}	0.84	0.4
u_{vr}	0.74	0.8	y_{vr}	1.1	1.2

q = 1000

	Mean ($\times 10^{-3}$)	Standard Deviation ($\times 10^{-3}$)		Mean	Standard Deviation
u_{hl}	0.68	0.05	y_{hl}	0.22	0.02
u_{hr}	0.15	0.2	y_{hr}	0.020	0.002
u_{vl}	0.040	0.003	y_{vl}	0.011	0.0006
u_{vr}	0.017	0.003	y_{vr}	0.0043	0.001

q = 4×10^5

	Mean ($\times 10^{-3}$)	Standard Deviation ($\times 10^{-3}$)		Mean	Standard Deviation
u_{hl}	0.91	0.1	y_{hl}	0.23	0.03
u_{hr}	0.26	0.04	y_{hr}	0.021	0.003
u_{vl}	0.056	0.006	y_{vl}	0.0091	0.001
u_{vr}	0.031	0.006	y_{vr}	0.0024	0.0007

Table 6.6 Integration of Scaled Squared Signal of LQG Controllers Response to a Horizontal Tap at Left End of Shaft with Added Mass

q = 50

	Mean ($\times 10^{-3}$)	Standard Deviation ($\times 10^{-3}$)		Mean	Standard Deviation
u_{hl}	0.95	0.05	y_{hl}	0.29	0.02
u_{hr}	0.31	0.03	y_{hr}	0.043	0.003
u_{vl}	0.056	0.003	y_{vl}	0.019	0.001
u_{vr}	0.044	0.005	y_{vr}	0.013	0.002

q = 100

	Mean ($\times 10^{-3}$)	Standard Deviation ($\times 10^{-3}$)		Mean	Standard Deviation
u_{hl}	1.0	0.06	y_{hl}	0.24	0.02
u_{hr}	0.36	0.04	y_{hr}	0.038	0.003
u_{vl}	0.052	0.004	y_{vl}	0.012	0.0009
u_{vr}	0.036	0.005	y_{vr}	0.0070	0.001

q = 500

	Mean($\times 10^{-3}$)	Standard Deviation ($\times 10^{-3}$)		Mean	Standard Deviation
u_{hl}	1.55	0.2	y_{hl}	0.17	0.02
u_{hr}	0.97	0.3	y_{hr}	0.044	0.01
u_{vl}	0.080	0.01	y_{vl}	0.0067	0.0008
u_{vr}	0.10	0.02	y_{vr}	0.0057	0.001

Table 6.7 Integration of Scaled Squared Signal of DSMC Controller Response to a Horizontal Tap at Left End of Shaft with Added Mass

	Mean ($\times 10^{-3}$)	Standard Deviation ($\times 10^{-3}$)		Mean	Standard Deviation
u_{hl}	1.14	0.06	y_{hl}	0.25	0.02
u_{hr}	0.58	0.03	y_{hr}	0.12	0.009
u_{vl}	0.054	0.004	y_{vl}	0.014	0.001
u_{vr}	0.029	0.004	y_{vr}	0.0056	0.0007

Table 6.8 Integration of Squared Signal of DSMC Controller with Switched Surface Response to a Horizontal Tap at Left End of Shaft with Added Mass

	u_{hl}	u_{hr}	u_{vl}	u_{vr}
Built-In Compensators	0.0796	0.153	0.207	0.169
LQG ($q = 2.5$)	0.0115	0.0188	0.0174	0.0211
LQG ($q = 1000$)	0.00603	0.0145	0.00979	0.00969
LQG ($q = 4 \times 10^5$)	0.0110	0.0206	0.0102	0.0104
DSMC-PI ($q = 50$, $r = 50$)	0.00823	0.0165	0.0189	0.0157
DSMC-PI ($q = 100$, $r = 50$)	0.00948	0.0197	0.0227	0.0178
DSMC-PI ($q = 500$, $r = 50$)	0.137	0.267	0.176	0.179

	y_{hl}	y_{hr}	y_{vl}	y_{vr}
Built-In Compensators	21.8	26.5	49.3	55.4
LQG ($q = 2.5$)	13.2	14.7	18.7	22.8
LQG ($q = 1000$)	1.40	1.92	3.11	3.33
LQG ($q = 4 \times 10^5$)	1.20	1.71	2.76	2.55
DSMC-PI ($q = 50$, $r = 50$)	2.21	2.70	5.79	5.10
DSMC-PI ($q = 100$, $r = 50$)	1.73	2.17	4.88	4.13
DSMC-PI ($q = 500$, $r = 50$)	11.8	16.2	21.7	22.3

Table 6.9 Variance of Control Action (Top) and Outputs (Bottom) with Matched Noise Disturbance

precisely but was too aggressive and the output variance was higher than with the lower values of q.

The DSMC-PI controller with a switched sliding surface for both the horizontal and vertical controllers could not be run on the hardware available since the computations that were required between each sample could not be performed in time.

6.7 Rotating Shaft

A strip of lead weighing 235g was wrapped around the shaft at a position left of centre approximately doubling the mass of the shaft. This produced an imbalance in the shaft in both the left to right sense and circumferentially as well as added mass to the shaft. A DC motor was used to spin the shaft using a rubber band around the center of the shaft to a pulley on the motor. A friction drive pulled the shaft in an approximate horizontal

direction and a variable voltage supply was used to control the motor speed. A strobe light was used to measure the speed of the shaft and the DC voltage was adjusted to produce a speed of 10,000 rpm. Once the speed was reached, the inputs and outputs of the plant were recorded for a few seconds. This process was repeated for each of the controllers. The data was scaled and the variance of a one second window of data is shown in Table 6.10.

The imbalancing mass and simple drive method was used to produce repeatable disturbances as well as test the performance under a rotating condition. The rotation causes some dynamic coupling between the horizontal and vertical axes due to the gyroscopic effect so a control action taken in one axis will result in a position change in both axes. The model identified in Chapter 4 and used to design the LQG and DSMC controllers assumes that there is no coupling between the axes.

The results show that the LQG controllers with q set to 1000 or 4×10^5 have a lower variance than all of the other controllers. The DSMC-PI controllers used more control action than the other controllers but did not perform as well.

6.8 Test Results Summary

This chapter presented the results of tests performed on the magnetic bearing apparatus with the built-in compensators, three tunings of the LQG controller, three tunings of the DSMC-PI controller and a switched surface DSMC-PI controller. The tests verify the tuning design of the LQG and DSMC-PI controllers showing that there is a trade-off between the amount of output deviation due to a disturbance versus the amount of control action used.

	u_{hl}	u_{hr}	u_{vl}	u_{vr}
Built-In Compensators	0.000935	0.00207	0.00102	0.001425
LQG ($q = 2.5$)	0.00136	0.00364	0.00113	0.00359
LQG ($q = 1000$)	0.00237	0.00729	0.00339	0.00519
LQG ($q = 4 \times 10^5$)	0.00267	0.00721	0.00290	0.00522
DSMC-PI ($q = 50$, $r = 50$)	0.00471	0.0162	0.00510	0.00429
DSMC-PI ($q = 100$, $r = 50$)	0.00352	0.0123	0.00713	0.00455
DSMC-PI ($q = 500$, $r = 50$)	0.00813	0.0147	0.0104	0.0107

	y_{hl}	y_{hr}	y_{vl}	y_{vr}
Built-In Compensators	0.467	0.975	0.418	1.04
LQG ($q = 2.5$)	0.477	2.25	0.448	1.48
LQG ($q = 1000$)	0.271	0.456	0.531	0.704
LQG ($q = 4 \times 10^5$)	0.195	0.377	0.420	0.710
DSMC-PI ($q = 50$, $r = 50$)	0.652	1.39	0.891	0.875
DSMC-PI ($q = 100$, $r = 50$)	0.430	0.864	1.00	0.718
DSMC-PI ($q = 500$, $r = 50$)	0.414	0.516	0.832	0.713

Table 6.10 Variance of Control Action (Top) and Outputs (Bottom) with a Rotating Shaft

In general, the two digital controllers performed better than the built-in compensators in terms of the amount of output deviation measured due to disturbances. The LQG controller with $q = 2.5$ responded slowly to disturbances while tunings with $q = 1000$ and $q = 4 \times 10^5$ responded quite similar to each other. There was little gain in performance for the increase in control action used by the $q = 4 \times 10^5$ tuning. The three DSMC-PI controllers generally did not perform quite as well as the LQG controllers. The tuning with $q = 500$ seemed to be too aggressive since there was a degradation in the performance with the increase in control action used when compared to the $q = 100$ tuning. The DSMC-PI controller reduced the deviation of the shaft due to a tap disturbance better than the other controllers. The DSMC-PI controller generally used more control energy. The DSMC-PI controller, however, may prove to be more robust in the presence of specific disturbances than the LQG controller.

One explanation for the relatively lower performance of the DSMC controller is that there is a one sample delay from the controller to the input to the apparatus which must degrade the performance since the controller must wait for one sample before it can respond to a measured disturbance. All of the controllers showed good robustness to changes in the plant dynamics shown by the taps on the shaft with added mass and rotating the shaft with an added mass. The PI component of the DSMC-PI controller did not have a significant effect in rejecting disturbances but served to attain a zero steady state error.

Chapter 7
Summary and Recommendations

7.1 Summary

This thesis provided methods for designing digital controllers for magnetic bearing systems. The designed controllers were experimentally tested and compared.

The controllers were designed for a laboratory scale magnetic bearing apparatus which operates on the same principles and has the same characteristics as industrial applications such as in compressor stations. Several different methods of modeling the apparatus were attempted. An analysis of the physical principles of the apparatus yielded an unreliable open loop model. The apparatus contains built-in compensators to levitate the shaft that were utilized to measure a closed loop frequency response. The response was modeled but the open loop model derived was parametric in the compensators and thus unsuitable for controller design.

An accurate model was produced using the parameter estimation method. This used input and output data to identify a model of the plant with the lowest error in a least squares sense. The resonance of the identified model was modified to reduce the damping and reflect the true apparatus more accurately. A simulation demonstrating this difficulty in identifying a resonance was presented. The result of the modeling was a two input, two output 16 state model for each of the horizontal and vertical axes. This method of modeling a magnetic bearing appears to be novel.

Two digital controllers were designed based on these models. A cost function was formulated to weight the output variation versus the control action in the design of an LQG controller. In a similar manner, an optimal sliding surface for a DSMC was designed based on a trade-off between the output variation and the level of control action. This is a new implementation for this control law and it was stable with the relatively slow sampling rate. A Kalman filter was designed to estimate the system states. These state estimates were used for both the DSMC and LQG controllers. The implementation of the DSMC with a Kalman filter for estimating the states produced an algebraic loop requiring a delay to be inserted into the controller. A PI controller was added to the DSMC to improve the tracking performance. As a final modification, a DSMC controller was designed with a choice of sliding surface dependant on the shaft position. The intention was to apply a more aggressive control action when one end of the shaft had a large deviation from the zero-position. The large number of parameters made this controller difficult to tune and due to computational speed, the computer could not execute this controller for both axes at the same time. This switched sliding surface design for a magnetic bearing is a novel approach.

The designed controllers as well as the built-in compensators were tested by tapping the shaft with a pendulum, adding mass to the shaft and tapping it with a pendulum, adding noise to the control inputs, and rotating the shaft with an imbalance. All of these tests examined the performance of the controllers and verified the tuning intentions. It was found that the LQG controllers with the more aggressive tuning generally performed the best in reducing shaft deviations. The built-in compensators tended to oscillate while the DSMC-

PI controllers performed almost as well as the LQG controllers. The DSMC-PI controller had the lowest shaft deviation following a tap disturbance to the shaft. The switched surface controller used a more aggressive control action but tended to oscillate. The PI component of the DSMC-PI controller produced accurate tracking performance.

The delay in the DSMC must degrade the performance of the controller since the control action is delayed one sample in response to a measured output change. A faster sampling rate would reduce this effect and presumably enhance the performance of the controller. One benefit of this delay is that the optimal sliding surface can be easily designed with a relative weight between output variation and control action.

7.2 Recommendations

The work presented in this thesis was based on a fixed model of a non-rotating system. An extension of this work would be an adaptive controller operating on a rotating system. The following items are of research interest:

- A four input, four output model would be identified using the parameter estimation method in the same way as the modeling in this thesis.
- A controller would be designed using this model.
- A recursive least squares estimation algorithm would be implemented to update the model while the controller is active. This would model all of the changes in dynamics due to rotation.

- The controller would be redesigned on-line using the updated model.

A fast computer would be required to perform all of the required computations. A faster sampling rate would also provide better input resolution and presumable better control performance.

Bibliography

Ahrens, M., L. Kučera, R. Larsonneur, "Performance of a Magnetically Suspended Flywheel Energy Storage Device", *IEEE Transactions on Control System Technology*, Vol. 4, No. 5, pp. 494-501, September, 1996

Anderson, B. D. D. and J. B. Moore, *Optimal Control: Linear Quadratic Methods*, Prentice-Hall Inc., 1990

Åström, K. J., and T. Hägglund, "PID Control - Theory, Design and Tuning", *2nd ed.*, *Instrument Society of America*, Research Triangle Park, NC, 1995

Bleuler, H., D. Visher, G. Schweiter, A. Traxler and D. Zlatnik, "New Concepts for Cost-Effective Magnetic Bearing Control", *Automatica*, Vol. 30 No. 5, pp. 871-876, 1994

Charara, A., J. De Miras, and B. Caron, "Nonlinear Control of a Magnetic Levitation System Without Premagnetization", *IEEE Transactions on Control Systems Technology*, Vol. 4, No. 5, pp. 513-523, September, 1996

DeCarlo, R. A., S. H. Żak and S. V. Drakunov, "Variable Structure, Sliding-Mode Controller Design", *The Control Handbook*, Edited by W. S. Levine, CRC Press Inc., pp. 941-951, 1996

Dahleh, M. A. and I. J. Diaz-Bobillo, *Control of Uncertain Systems*, Prentice Hall Inc., 1995

DeSantis, R. M., "An Adaptive PI/Sliding Mode Controller for a Speed Drive", *ASME Journal of Dynamics Systems, Measurement, and Control*, Vol. 111, pp. 409-415, 1989

Edwards, C., and S. K. Spurgeon, "On the Development of Discontinuous Observers", *International Journal of Robust and Nonlinear Control*, Vol. 59, No. 5, pp.1211-1229, 1994

Fialho, I., and G. Balas, "Adaptive Vehicle Suspension Design Using LPV Methods", *Proc. IEEE Conf. on Precision and Control*, Tampa, Florida, USA, pp.469-474, December 1998

Furuta, K., "Sliding Mode Control of a Discrete System", *Systems and Control Letters*, Vol. 14, pp. 145-152

Herzog, R. H., P. Buhler, and C. Gahler, "Unbalance Compensation Using Generalized Notch Filters in the Multivariable Feedback of Magnetic Bearings", *IEEE Transactions on Control Systems Technology*, Vol. 4, No. 5, pp. 580-586, September, 1996

Humpris, R. R., R. D. Kelm, D. W. Lewis and P. E. Allaire, "Effect of Control Algorithms on Magnetic Journal Bearing Properties", *AMSE Journal of Engineering for Gas Turbines and Power*, Vol. 108, pp.624-632,October 1986

Knospe, C. K., and Collins, E., "Introduction to the Special Issue on Magnetic Bearing Control", *IEEE Transactions on Control Systems Technology*, Vol. 5, No. 5, pp.481-483, September 1996

Lee, C., Y. Ha, C. Kim and C. Joh, "Modal Testing and Parameter Identification of Active Magnetic Bearing System", *ASME Design Engineering Technical Conference*, DE-Vol. 3-Part B, 1995

Lewis, A. S., A. Sinha and K. W. Wang, "Sliding Mode Output Feedback Control of a Flexible Rotor Via Magnetic Bearings", *International Gas Turbine & Aeroengine Congress & Exhibition*, Stockholm, Sweeden, June 2-5 1998

Li, W. and J. H. Lee, "Frequency-Domain Closed-Loop Identification of Multivariable Systems for Feedback Control", *AIChE Journal*, Vol. 42, No. 10, pp. 2813-2827, October 1996

Ljung, L., *System Identification - Theory for the User*, Prentice Hall, 1999

Lum, K.-Y. L., V. T. Coppola, and D. S. Bernstein, "Adaptive Autocentering Control for an Active Magnetic Bearing Supporting a Shaft with Unknown Mass Imbalance", *IEEE Transactions on Control Systems Technology*, Vol. 4, No. 5,pp. 587-597, September, 1996

Magnetic Moments, *MBC 500 Magnetic Bearing System Operating Instructions*, 1997

The Math Works, *Using Matlab, Ver. 5*, The Math Works, 1996

Matsumura, F., T. Namerikawa, K. Hagiwara, and M. Fujita, "Application of Gain Scheduled H_∞ Robust Controllers to a Magnetic Bearing", *IEEE Transactions on Control Systems Technology*, Vol. 4, No. 5, pp. 484-492, September, 1996

Matsumura, F. and T. Yoshimoto, "System Modeling and Control Design of a Horizontal-Shaft Magnetic-Bearing System", *IEEE Transactions on Magnetics*, Vol. Mag-22, No. 3,pp. 196-203, May 1986

Mizuno, T., K. Araki, and H. Bleuler, "Stability Analysis of Self-Sensing Magnetic Bearing Control", *IEEE Transactions on Control Systems Technology*, Vol. 4, No. 5, pp. 572-579, September 1996

Mohamed, A. M., and I. Busch-Vishniac, "Imbalance Compensation and Automation Balancing in Magnetic Bearing Systems Using the Q-Parameterization Theory", *IEEE Transactions on Control Systems Technology*, Vol. 3, No. 2, pp. 202-210, June 1995

Noh, M. D. and E. H. Maslen, "Self-Sensing Magnetic Bearings Using Parameter Estimation", *IEEE Transactions on Instrumentation and Measurement*, Vol. 46, No. 1, pp. 45-50, February 1997

Nonami, K. and T. Ito, "μ Synthesis of Flexible shaft-Magnetic Bearing Systems", *IEEE Transactions on Control Systems Technology*, Vol. 4, No. 5, pp. 503-512, September, 1996

Nonami, K. and H. Yamaguchi, "Robust Control of Magnetic Bearing Systems by Means of Sliding Mode Control", *Proceedings to the 3rd International Symposium on Magnetic Bearings*, Alexandria, Virginia, USA, pp. 537-546, 1992

Phan, M., and R. W. Longman, "System Identification from Closed-Loop Data with Known Output Feedback Dynamics", AIAA *Journal of Guidance, Control, and Dynamics*, Vol. 17, No. 4, pp. 661-669, July-August, 1994

Pieper, J. K. and B. W. Surgenor, "Discrete Sliding Control of a Coupled-Drives Apparatus with Optimal Sliding Surface and Switching Gain", *IEE Proceedings-D*, Vol. 140, No. 2, pp 70-78, March 1993

Quanser Consulting Inc., *WinCon 3.0.2a*, 1998

Queiroz, M. S., and D. M. Dawson, "Nonlinear Control of Active Magnetic Bearings: A Backstepping Approach", *IEEE Transactions on Control Systems Technology*, Vol. 4, No. 5, pp.545-552, September, 1996

Rundell, A. E., S. V. Drakunov, and R. A. DeCarlo, "A Sliding Mode Observer and Controller for Stabilization of Rotational Motion of a Vertical Shaft Magnetic Bearing", *IEEE Transactions on Control Systems Technology*, Vol. 4, No. 5, pp.598-608, September 1996

Sheu, G. J., C. D. Yang and S. M. Yang, "Experiment-Aided Controller Design of Rotor Systems with a Magnetic Bearing", *ASME International Gas Turbine and Aeroengine Congress and Exposition*, June 5-9, 1995

Sivrioglu, S. and K. Nonami, "Sliding Mode Control with Time-Varying Hyperplane for AMB Systems", *IEEE/ASME Transactions on Mechatronics*, Vol. 3, No. 1, pp. 51-59, March 1998

Skogestad, S. and I. Postlethwaite, *Multivariable Feedback Control*, John Wiley and Sons, 1996

Slotine, J. J. E., J. K. Hedrick, and E. A. Misawa, "On Sliding Observers for Nonlinear Systems", ASME *Journal of Dynamic Systems, Measurement, and Control*, Vol. 109, pp.245-252, September, 1987

Slotine, J.J. E. and W. Li, Applied Nonlinear Control, Prentice Hall, 1991

Smith, R. D. and W. F. Weldon, "Nonlinear Control of a Rigid Rotor Magnetic Bearing System: Modeling and Simulation with Full State Feedback", *IEEE Transactions on Magnetics*, Vol. 31, No. 2, pp. 973-980, March 1995

Suzuki, Y., "Acceleration Feedforward Control for Active Magnetic Bearing Systems Excited by Ground Motion", *IEE Proceedings - Control Theory and Applications*, Vol. 145, No. 2, pp. 113-118, March 1998

Tian, H., and K. Nonami, "Discrete-Time Sliding Mode Control of Flexible Rotor-Magnetic Bearing Systems", *International Journal of Robust Control and Nonlinear Control*, Vol. 6, pp.609-632, 1996

Utkin, V. I., "Variable Structure Systems with Sliding Modes", *IEEE Transactions on Automatic Control*, Vol. AC-22, No, 2, pp. 212-222, April 1977

Vidolov, B., C. Mélin, J. De Miras and A. Charara, "Two-Rule-Based Fuzzy Logic Control and Sliding Mode Control of an Active Magnetic Bearing", *IEEE International Conference on Fuzzy Systems*, Sep 8-11, 1996

Walcott, B. L., and S. H. Zak, "State Observation of Nonlinear Uncertain Dynamical Systems", *IEEE Transactions on Automatic Control*, Vol. AC-32, No. 2, pp. 166-169, February, 1987

Appendix A
Model Matrices

$$A_{hl} = A_{hr} = \begin{bmatrix} 0.98505 & 1 & 0 & 0 & 0 & 0 & 0 & 0 \\ 0.11763 & 0 & 1 & 0 & 0 & 0 & 0 & 0 \\ -0.17539 & 0 & 0 & 1 & 0 & 0 & 0 & 0 \\ -0.018721 & 0 & 0 & 0 & 1 & 0 & 0 & 0 \\ 0.3181 & 0 & 0 & 0 & 0 & 1 & 0 & 0 \\ 0.278 & 0 & 0 & 0 & 0 & 0 & 1 & 0 \\ -0.025524 & 0 & 0 & 0 & 0 & 0 & 0 & 1 \\ -0.45605 & 0 & 0 & 0 & 0 & 0 & 0 & 0 \end{bmatrix}^T$$

$$B_{hl} = B_{hr} = \begin{bmatrix} 1 & 0 & 0 & 0 & 0 & 0 & 0 & 0 \end{bmatrix}^T$$

$$H_{hl} = \begin{bmatrix} 0.017438 & 0.00066827 \\ 0.0087623 & -0.002571 \\ 0.013057 & -0.004487 \\ 0.010474 & 0.0023162 \\ 0.0024121 & 0.016418 \\ -0.006399 & 0.017365 \\ -0.0046465 & 0.0042347 \\ 0.020481 & -0.021079 \end{bmatrix}^T \qquad H_{hr} = \begin{bmatrix} -0.0099798 & 0.032525 \\ -0.000936 & 0.0061558 \\ 0.010106 & 0.00085146 \\ 0.014508 & -0.0025218 \\ 0.0092223 & 0.0082346 \\ 0.0075479 & 0.0055543 \\ -0.0027971 & 0.00062272 \\ -0.011667 & 0.0089137 \end{bmatrix}^T$$

$$D_{hl} = D_{hr} = 0_{2\times 2}$$

$$A_{vl} = A_{vr} = \begin{bmatrix} 0.92468 & 1 & 0 & 0 & 0 & 0 & 0 & 0 \\ 0.13536 & 0 & 1 & 0 & 0 & 0 & 0 & 0 \\ -0.11673 & 0 & 0 & 1 & 0 & 0 & 0 & 0 \\ -0.02638 & 0 & 0 & 0 & 1 & 0 & 0 & 0 \\ 0.29848 & 0 & 0 & 0 & 0 & 1 & 0 & 0 \\ 0.3043 & 0 & 0 & 0 & 0 & 0 & 1 & 0 \\ -0.0055853 & 0 & 0 & 0 & 0 & 0 & 0 & 1 \\ -0.49169 & 0 & 0 & 0 & 0 & 0 & 0 & 0 \end{bmatrix}^T$$

$$B_{vl} = B_{vr} = \begin{bmatrix} 1 & 0 & 0 & 0 & 0 & 0 & 0 & 0 \end{bmatrix}^T$$

$$H_{vl} = \begin{bmatrix} -0.025481 & 0 \\ 0.037874 & 0 \\ 0.018788 & 0 \\ 0.0088599 & -0.0023034 \\ 0.013175 & 0.011782 \\ 0.017573 & -0.010688 \\ 0.0059225 & -0.011246 \\ -0.013031 & -0.0080531 \end{bmatrix}^T \qquad H_{vr} = \begin{bmatrix} -0.004014 & 0 \\ 0.018508 & 0 \\ -0.0009463 & 0 \\ -0.0080458 & -0.011723 \\ -0.014791 & 0.033134 \\ -0.020473 & 0.028162 \\ -0.0036804 & 0.0091269 \\ 0.023352 & 0.035807 \end{bmatrix}^T$$

$$D_{vl} = D_{vr} = 0_{2\times 2}$$